Geophys. J. Int. (1994) **116,** 421–446

Computation of synthetic seismograms and their partial derivatives for heterogeneous media with arbitrary natural boundary conditions using the Direct Solution Method

Robert J. Geller and Takao Ohminato*

Department of Earth and Planetary Physics, Faculty of Science, Tokyo University, Yayoi 2-11-16, *Bunkyo-ku, Tokyo* 113, *Japan*

Accepted 1993 July 19. Received 1993 July 15; in original form 1993 April 22

SUMMARY

A new method is presented for calculating synthetic seismograms and their partial derivatives for laterally and vertically heterogeneous media with arbitrary natural boundary conditions. The formulation is derived by adding appropriate surface integrals to the weak form (Galerkin formulation) of the elastic equation of motion to enforce the natural boundary and continuity conditions, and inhomogeneous boundary conditions. Results applicable to media consisting of a combination of fluid and solid regions are presented. The method is called the Direct Solution Method (DSM) (Geller *et al.* 1990c) because the synthetic seismograms and partial derivatives are computed directly by solving a system of linear equations. In contrast, almost all previous applications of Galerkin methods in seismology have first computed the modes of free oscillation, and only then computed the synthetic seismograms and partial derivatives by summing the modes. As an example of the application of our method, we calculate synthetic seismograms for heterogeneous media which are terminated at the bottom by a thin homogeneous layer with a radiation (energy-absorbing) boundary condition.

This method is well suited to computing the quantities necessary to perform linearized inversion for earth structure with respect to a laterally heterogeneous earth model (Geller & Hara 1993). It thus becomes possible to formulate iterative linearized waveform inversion for laterally heterogeneous earth structure on a local and regional scale following the same basic approach used by Hara, Tsuboi & Geller (1993) to invert waveform data for global laterally heterogeneous structure.

Key words: Direct Solution Method, partial derivatives, synthetic seismograms.

1 INTRODUCTION

Inverting seismic-waveform data to determine earth structure is an important topic in seismology at all distance scales (global, regional, local and exploration). As the perturbation to the synthetic seismogram is a non-linear functional of the model perturbation, such inversion is inherently a non-linear problem; the most practical approach appears to be iterative linearized inversion, with the 3-D model determined by each iteration serving as the 3-D starting model for the next iteration (Geller & Hara 1993). To conduct iterative linearized inversion for 3-D earth structure it is necessary to be able to calculate synthetic seismograms accurately for an arbitrary 3-D earth model. This paper presents methods which are well suited to making such calculations.

Hara, Tsuboi & Geller (1993) conducted iterative linearized waveform inversion of long-period (200–400 s) surface-wave data to determine the 3-D *S*-wave velocity structure of the upper mantle on a global scale. (The basic approach used by Hara *et al.* can be applied to body-wave data as well as surface-wave data.) Hara *et al.* (1993) used the Direct Solution Method (DSM) (Geller *et al.* 1990c) to calculate the synthetic seismograms and their partial derivatives. The DSM is based on solving the *weak form* (Galerkin formulation) of the elastic equation of motion. The DSM, which is explained in detail below, is so named because the solution is obtained by *directly solving* a system of linear equations, rather than by first introducing the unnecessary intermediate step of calculating modes of free

*Now at: Geological Survey of Japan, Higashi 1-1-3, Tsukuba-shi, Ibaraki-ken 305, Japan.

oscillation and then computing the synthetic seismograms by modal superposition.

It is desirable to be able to apply the same basic approach as Hara *et al.* (1993) to the inversion of waveform data from strong-motion seismology, exploration geophysics and local and regional seismic networks. However, the DSM was originally formulated for global-scale studies, and only free surface boundary conditions were considered. In contrast with global studies, the numerical models for regional or local studies must be terminated by artificial boundaries at the edge of the computational domain; spurious reflections from these artificial boundaries must be suppressed. In many instances exact or approximate energy-absorbing boundary conditions at such artificial boundaries can be formulated as *natural boundary conditions*. (Note that a free surface boundary condition is a particular instance of a natural boundary condition.) This paper extends the DSM formulation to regions terminated by arbitrary natural boundary conditions. Thus the DSM can be used to calculate synthetic seismograms for media terminated by many previously proposed energy-absorbing boundary conditions, and for any energy-absorbing boundary conditions which might be proposed in the future if they are natural boundary conditions.

1.1 Weak and strong forms of partial differential equations

The DSM computes synthetic seismograms and their partial derivatives by solving the weak form of the elastic equation of motion. Discussions of the concept of weak and strong forms of partial-differential equations and demonstrations of their equivalence are relatively common in applied mathematics and engineering. Detailed discussions from the standpoint of numerical computation are given by Strang & Fix (1973) and Johnson (1987). A more rigorous mathematical discussion is given by Dautray & Lions (1988, Chapters 7, 12 and 18).

The terms 'strong form' and 'weak form' are used because the former requires the solutions explicitly to satisfy stringent conditions (both continuity of displacement and continuity of traction in the case of the elastic equation of motion), whereas the latter requires less stringent conditions to be explicitly satisfied (continuity of displacement only in the case of the elastic equation of motion). Continuity of traction, as shown in the following, is a natural continuity condition which is automatically satisfied by the weak-form solutions despite its not being explicitly imposed. Natural boundary conditions are also, as shown below, automatically satisfied by the weak-form solutions without their having to be explicitly imposed.

The overwhelming majority of published work on solving 'the' elastic equation of motion has concentrated on solving the strong form of the elastic equation of motion (e.g. Kennett 1983; Chapman & Orcutt 1985). Also, almost all previous applications of the weak form of the elastic equation of motion have been limited to the calculation of modes of free oscillation and the computation of synthetic seismograms by modal superposition. The study of Olson, Orcutt & Frazier (1984), who presented direct solutions of the weak form of the elastic equation of motion for flat-layered laterally homogeneous media, is a notable exception.

1.2 Contents of this paper

Section 2 begins by defining the weak and strong forms of the elastic equation of motion for media with either fixed or free boundary conditions, and showing that they are equivalent. We then derive the weak form of the elastic equation of motion for media with arbitrary homogeneous natural boundary conditions. We next show how to include inhomogeneous traction and displacement boundary conditions (including a dislocation) as natural boundary conditions in the weak form. We also present the weak form of the equation of motion for the partial derivatives of the synthetic seismograms with respect to the model parameters (i.e. the first-order Born approximation).

In Section 3 we derive the weak form of the equation of motion for a medium containing both fluid and solid regions, using (a quantity proportional to) the pressure change as the dependent variable in the fluid regions and the displacement as the dependent variable in the solid regions. Continuity of normal displacement and continuity of normal traction at the fluid–solid boundaries are enforced by adding surface integrals to the weak-form operator, so that these conditions become natural continuity conditions.

In Section 4 we present the systems of linear equations obtained from the results presented in Sections 2 and 3. We present the Galerkin weak form of the equation of motion, which is obtained by using the same set of functions as both weight functions and trial functions. We also discuss the relation between the DSM and modal superposition methods. The computational requirements of the DSM are briefly discussed.

In Section 5, we give numerical results for four relatively simple test calculations of synthetic seismograms. In all four cases a radiation boundary condition is specified at the lower boundary of the medium. Two of the four test calculations are for a laterally homogeneous medium: a 2-D (line source) calculation in Cartesian coordinates and a 3-D (point source) calculation in cylindrical coordinates. The remaining two test calculations are for *SH*-wave propagation in a 2-D laterally heterogeneous medium (a sedimentary basin of variable thickness overlying a higher velocity layer). The first such calculation is for a line source within the medium, whereas the second is for a plane wave vertically incident from below. We compare the results for the first case to those computed using two other methods, and show that there is good agreement. We also present numerical tests of the degradation in accuracy caused by the truncation of coupling between more distant wavenumbers; these tests demonstrate the trade-off between accuracy and CPU time. Although the numerical examples are all for isotropic media, the methods in this paper are applicable to a general anisotropic medium.

The choice of trial functions, the bookkeeping required to order the trial functions so that the bandwidth of the matrices is minimized, and an overview of the evaluation of the matrix elements are discussed in Appendix A. The details required to formulate radiation boundary conditions for certain media as natural boundary conditions are discussed in Appendix B.

1.3 Previous work

The computation of synthetic seismograms is one of the most fundamental problems in seismology. This important

topic has been discussed in literally thousands of previous publications; it is both impossible and unnecessary to summarize this work here. However, we present a brief discussion of previous work, with particular emphasis on its relation to the methods considered in this paper.

In a laterally homogeneous isotropic medium, separation of variables can be applied, and the elastic equation of motion can be transformed to a coupled set of ordinary differential equations. Many different approaches have been used to solve the resulting set of coupled ordinary differential equations. This large body of work may be divided into two main families. The first consists of methods that use propagator-matrix techniques (i.e. Haskell 1953; Thomson 1950), of which the reflectivity method (Fuchs & Müller 1971) is perhaps the best known. The monograph by Kennett (1983) and the review by Chapman & Orcutt (1985) extensively discuss many methods based on propagator-matrix techniques.

A second class of methods uses purely numerical techniques (finite element, finite difference, etc.) to solve the ordinary differential equations. These methods, generally described as 'low-frequency methods', have the advantage of being able to treat arbitrarily vertically heterogeneous media; they are not limited to a stack of homogeneous layers. These methods also have the disadvantage (as compared with propagator-matrix techniques) of requiring computational effort roughly proportional to the cube of the maximum frequency. However, the distinction between propagator-matrix methods and low-frequency methods is artificial. Although the computational effort for propagator-matrix methods is a function only of the number of layers and is essentially frequency independent, the number of layers must be increased with increasing frequency if realistic results are to be obtained.

Among the most notable examples of low-frequency methods is that of Alekseev & Mikhailenko (1976; 1980) and Mikhailenko (1985), based on the finite-difference method (FDM). Olson, Orcutt & Frazier (1984) derive a set of discrete equations using finite-element method (FEM) rather than FDM. However, as Olson *et al.* (1984) use linear splines as the trial functions, their actual calculations are essentially equivalent to Alekseev & Mikhailenko's FDM calculations. Both Alekseev & Mikhailenko (1976; 1980) and Olson *et al.* (1984) solved the problem in the t–k (time–wavenumber) domain. Other work on low-frequency methods includes that of Spudich & Ascher (1983), who use the collocation method, and Korn (1987), who developed a frequency-domain version of the Alekseev–Mikhailenko method.

A number of methods have been developed for calculating synthetic seismograms in laterally heterogeneous media. Asymptotic ray theory and the Gaussian beam method (Červený 1983), which are computationally efficient but use many approximations, are well suited to modelling high-frequency waves. Wave theoretical approaches have been applied to media consisting of homogeneous layers with irregular interfaces (Aki & Larner 1970; Bouchon & Aki 1977a; 1977b; Kohketsu 1987a; 1987b). However, the real Earth has not only sharp discontinuities, but also gradual variations in seismic velocities. Purely numerical methods, such as FDM (e.g. Boore 1970; Kelly *et al.* 1976) or FEM (e.g Smith 1975; Marfurt 1984), can be applied to arbitrarily heterogeneous media, but require extensive computations. Kosloff & Baysal (1982), and many later papers by Kosloff and his colleagues, have presented applications of the pseudo-spectral method.

1.4 Radiation boundary conditions

One of the problems in calculating synthetic seismograms for local or regional-scale problems is contamination due to artificial reflections from the edge of the computational domain. It is clearly desirable to develop boundary conditions which eliminate artificial reflections generated by these numerical boundaries; many previous workers have considered this question.

Lysmer & Kuhlemeyer (1969) use viscous damping, but their boundary condition cannot eliminate S waves perfectly. Smith (1974) uses the FEM and takes the average of two different solutions which satisfy fixed and free boundary conditions, respectively. The paraxial wave equation is widely used in finite-difference schemes as an approximate method for implementing non-reflecting boundaries (Clayton & Engquist 1977; Engquist & Majda 1977; 1979; Reynolds 1978). Kausel (1992) discusses the stability of such paraxial approximations.

Cerjan *et al.* (1985) adopt amplitude tapering (i.e. anelastic attenuation near the edge of the grid) and apply it to a pseudo-spectral method (Kosloff & Baysal 1982). Randall (1988) uses a reflectivity matrix to implement a radiation boundary condition for the scalar potential (Lindmann 1975) in an FDM scheme. Chang & McMechan (1989) apply Randall's approach to 3-D acoustic and elastic problems and present numerical examples for simple models. Higdon (1990) discusses the stability of radiation boundary conditions for the elastic equation of motion.

The Galerkin method has not previously been used by seismologists to solve the elastic equation of motion for media with radiation boundary conditions. Lysmer & Drake (1972) and Olson *et al.* (1984) imposed fixed, rather than radiation, boundary conditions at the base of the model. However, we show in the following that any natural boundary condition can easily be incorporated into the weak form of the elastic equation of motion by adding appropriate surface integrals to the basic formulation. In Appendix B we show that radiation boundary conditions for certain media can be formulated as natural boundary conditions which are rigorously satisfied by our numerical solutions. Our method for incorporating radiation boundary conditions in the elastic-wave equation is similar to that used by Fix & Marin (1978) and Goldstine (1982) for the scalar-wave equation (Helmholtz equation).

2 WEAK AND STRONG FORMS OF ELASTIC EQUATION OF MOTION

Except where otherwise stated, all of the results in this paper are derived in the frequency domain, for a Cartesian coordinate system. Summation over repeated dummy subscripts is implied throughout this paper when the subscripts refer to the physical (x, y, or z) coordinates, but not when the subscripts refer to abstract vector spaces (e.g. the vector space of trial functions). The effects of the Earth's rotation and self-gravitation are not included in this paper.

2.1 Strong form

Essentially all of the various numerical methods for solving the elastic equation of motion can be classified as particular implementations of the method of weighted residuals (MWR) (Finlayson 1972; Fletcher 1984). We represent the displacement, $\mathbf{u}(\mathbf{x})$, where u_i is the i component, and $\mathbf{x}$ is the spatial coordinate, as a linear combination of N linearly independent vector trial functions, $\{\phi_i^{(1)}(\mathbf{x}), \ldots, \phi_i^{(N)}(\mathbf{x})\}$,

$$u_i(\mathbf{x}) = \sum_{n=1}^{N} c_n \phi_i^{(n)}(\mathbf{x}), \tag{1}$$

where the expansion coefficients c_n become the unknowns. Note that both $u_i(\mathbf{x})$ and c_n are functions of the angular frequency, ω, but we do not write this dependence explicitly. For the moment we assume that the basis is a complete set, which may be infinite. The conditions that must be satisfied by the trial functions, $\phi_i^{(n)}$, are discussed in the following. Unless the representation in eq. (1) fortuitously is an exact solution, the equation of motion and boundary conditions will not be satisfied exactly. The resulting errors are called the domain residuals and boundary residuals, respectively.

Typically, the trial functions for strong form MWR implementations are chosen so that they satisfy either the boundary and continuity conditions, or the partial-differential equation, but not both (e.g. Fletcher 1984). In the former case the boundary residual is zero; such MWR implementations are called domain methods. In the latter case the domain residual is zero; such MWR methods are called boundary methods. Finally, if the trial functions satisfy neither the differential equation nor the boundary and continuity conditions, both the domain and boundary residuals will be non-zero; the resulting MWR methods, which are called mixed methods, will not be considered further here. The work of Aki & Larner (1970) is an example of an MWR boundary method, and that of Spudich & Ascher (1983) is an example of an MWR domain method.

The word 'weighted' identifies the key concept in MWR. We choose a set of N linearly independent vector weight functions $w_i^{(m)}$ $(m = 1, \ldots, N)$, which do not, in general, belong to the same function space as the trial functions, i.e. the continuity, differentiability and boundary conditions are in general different for the trial functions and the weight functions.

We multiply the domain residual (if we are considering a domain method) or the boundary residual (if we are considering a boundary method) by the weight functions and integrate to compute the weighted residuals. We then set the N weighted residuals to zero to obtain a set of N simultaneous linear equations for the expansion coefficients c_n.

For a domain method, the strong form of MWR for the elastic equation of motion in Cartesian coordinates in the frequency domain is

$$\int_V w_i^{(m)}[\rho\omega^2 u_i + (C_{ijkl}u_{k,l})_{,j} + f_i]\, dV = 0$$

$$(m = 1, \ldots, N), \tag{2}$$

where ρ is the density, and $C_{ijkl} = C_{jikl} = C_{klij}$ are the 21 independent elastic constants. Note that the elastic moduli C_{ijkl} are not restricted to being real or frequency independent; for example, the use of a superposition of standard linear solids to model anelastic attenuation (e.g. Liu, Anderson & Kanamori 1976) is entirely admissible. The subscript $,j$ denotes spatial differentiation with respect to the j coordinate, and f_i is the i component of the applied force. In eq. (2) the displacement u_i must be continuous, and the traction $(C_{ijkl}u_{k,l})n_j$ must be continuous in the n_j direction. As the displacement is an arbitrary superposition of the trial functions, each of the individual trial functions must satisfy these continuity conditions. Each individual trial function must also satisfy the boundary conditions, e.g. free or rigid boundary conditions. The weight functions, $w_i^{(m)}$, are not required to satisfy any differentiability, continuity, or boundary conditions; even δ functions are acceptable. We use the same number of weight functions and trial functions, so that the system of linear equations, eq. (2), will have a unique solution. For the moment we consider only media with homogeneous boundary conditions. Inhomogeneous boundary conditions (prescribed tractions or displacements) are discussed later.

2.2 Weak form

We now *define* a new operator, the weak form of the elastic equation of motion:

$$\omega^2 \int_V y_i^{(m)} \rho v_i\, dV - \int_V y_{i,j}^{(m)} C_{ijkl} v_{k,l}\, dV$$

$$= -\int_V y_i^{(m)} f_i\, dV. \quad (m = 1, \ldots, N). \tag{3}$$

To emphasize that we have not yet established any connection between the weak-form operator, eq. (3), and the strong-form operator, eq. (2), we designate the displacement by v_i rather than u_i, and the weight functions by $y_i^{(m)}$ rather than $w_i^{(m)}$. The number of trial functions is equal to the number of weight functions.

The requirement for the existence of the integrals in eq. (3) is that both the solution v_i and the weight functions $y_i^{(m)}$ must be continuous, but no continuity requirements are placed on the derivatives of these functions. We expand v_i in terms of N linearly independent vector trial functions, $[\psi_i^{(1)}(\mathbf{x}), \ldots, \psi_i^{(N)}(\mathbf{x})]$. At this point in our discussion we assume that the trial functions and weight functions are both complete sets, which may be infinite.

We represent the solution v_i as a linear combination of the trial functions

$$v_i(\mathbf{x}) = \sum_{n=1}^{N} d_n \psi_i^{(n)}(\mathbf{x}), \tag{4}$$

where the expansion coefficients d_n are the unknowns, and $\psi_i^{(n)}$ is the i component of the nth trial function.

Because, in general, the equivalence of the strong and weak solutions of partial-differential equations is a well-known result (e.g. Strang & Fix 1973, pp. 10–13; Johnson 1987, pp. 14–18; Dautray & Lions 1988, Ch. 7) the following discussion is a brief demonstration rather than a rigorous proof. To establish the relation between the weak-form operator defined in eq. (3) and the strong-form operator defined in eq. (2) we integrate eq. (3) by parts to

obtain

$$\int_V y_i^{(m)}[\rho\omega^2 v_i + (C_{ijkl}v_{k,l})_{,j} + f_i]\,dV - \int_S y_i^{(m)}[(C_{ijkl}v_{k,l})n_j]\,dS = 0 \quad (m = 1, \ldots, N), \tag{5}$$

where n_j is the outward unit normal vector.

As the weight functions $y_i^{(m)}$ are a complete set, their coefficients in eq. (5)—the terms in the square brackets—must be zero everywhere to guarantee that the right-hand side of eq. (5) is zero. The coefficient of $y_i^{(m)}$ in the volume integral must therefore be zero everywhere in the domain

$$[\rho\omega^2 v_i + (C_{ijkl}v_{k,l})_{,j} + f_i] = 0. \tag{6}$$

As this coefficient is in fact the strong form of the elastic equation of motion, we thus see that the strong form of the equation of motion is satisfied everywhere in the domain.

The preceding discussion assumed that the weak-form solutions were sufficiently differentiable to allow the integration by parts necessary to obtain eq. (5) from eq. (3). If, on the other hand, the trial functions do not satisfy the condition of continuity of traction, it might appear that the integration by parts cannot be performed. However, as was pointed out by Strang & Fix (1973, p. 11), trial functions whose tractions are not necessarily continuous (e.g. linear splines) can be obtained as the limit of a sequence of continuous functions whose tractions are continuous. Thus even when the integration by parts required to obtain eq. (5) cannot be rigorously performed, we can nevertheless regard this result as the limit of the result obtained for a sequence of admissible functions. This interpretation applies equally to other examples of integration by parts later in this section, but will not be repeated explicitly.

2.3 Natural and essential homogeneous boundary conditions

Using the same arguments applied in the preceding section to the volume integral in eq. (5), we can see that as the weight functions $y_i^{(m)}$ and the trial functions $\psi_i^{(n)}$ are complete sets, the integrand of the surface integral in eq. (5) must be zero everywhere on the boundary. This means that a free surface boundary condition

$$[(C_{ijkl}v_{k,l})n_j] = 0 \tag{7}$$

is satisfied automatically everywhere on the boundary, without its having to be imposed explicitly on the trial functions (Strang & Fix 1973, p. 12).

The free boundary condition, eq. (7), is an example of a natural boundary condition, i.e. a boundary condition that will automatically be satisfied by the weak-form solution regardless of whether or not it is explicitly satisfied by each of the individual trial functions. In contrast, a fixed boundary condition is an essential boundary condition, i.e. a boundary condition that will not be satisfied by the weak-form solution unless it is explicitly satisfied by *all* of the trial functions and all of the weight functions on the part of the boundary where the displacement is required to be equal to zero (e.g. Courant 1943).

For the elastic equation of motion *any* homogeneous boundary condition of the form

$$(C_{ijkl}v_{k,l})n_j - S_{ij}v_j = 0, \quad (i = 1, 2, 3) \tag{8}$$

where S_{ij} are constants that can vary with position along the boundary and with frequency, is a natural boundary condition. We give examples in Appendix B of how to obtain the coefficients S_{ij} so that eq. (8) will correspond to a radiation boundary condition. We now add a surface integral to eq. (3) to define a weak-form operator for which the natural boundary condition is eq. (8), rather than eq. (7):

$$\omega^2\int_V y_i^{(m)}\rho v_i\,dV - \int_V y_{i,j}^{(m)}C_{ijkl}v_{k,l}\,dV + \int_S y_i^{(m)}S_{ij}v_j\,dS = -\int_V y_i^{(m)}f_i\,dV \quad (m = 1, \ldots, N). \tag{9}$$

To demonstrate that the natural boundary condition for eq. (9) is eq. (8), we integrate by parts, obtaining

$$\int_V y_i^{(m)}[\rho\omega^2 v_i + (C_{ijkl}v_{k,l})_{,j} + f_i]\,dV - \int_S y_i^{(m)}[(C_{ijkl}v_{k,l})n_j - S_{ij}v_j]\,dS = 0 \quad (m = 1, \ldots, N). \tag{10}$$

As $y_i^{(m)}$ is arbitrary, the natural boundary condition eq. (8) will automatically be satisfied by the weak-form solutions obtained from eq. (9) unless all of the trial functions satisfy a fixed boundary condition.

It is surprising that weak-form operators of the form of eq. (9) have not previously been used to solve the elastic equation of motion for media with general natural boundary conditions of the form eq. (8), as such augmented weak-form operators have been widely used in other fields. For example, Fix & Marin (1978) and Goldstine (1982) defined similar augmented weak-form operators for the Helmholtz equation (i.e. acoustic wave equation). Also, adding surface integrals to the weak-form operator to impose inhomogeneous boundary conditions (e.g. prescribed tractions) is extensively discussed in engineering (e.g. Strang & Fix 1973, pp. 70–71; Johnson 1987, pp. 40–41). Finally, note that Courant's classic (1943) paper presented an example in which the natural boundary condition was varied by adding a boundary integral to a weak-form operator.

2.4 Natural and essential continuity conditions

Continuity of displacement is an essential continuity condition, i.e. a continuity condition that must be explicitly satisfied by the weak-form solutions. This condition must therefore be satisfied by each of the trial functions. In contrast, continuity of traction is a natural continuity condition, i.e. a continuity condition which is automatically satisfied by the weak-form solutions without its having to be explicitly satisfied by each of the trial functions (Strang & Fix 1973, p. 14). We verify this using, for simplicity, the weak-form operator defined in eq. (3) rather than the weak-form operator defined in eq. (9); however, the following argument applies equally to either case.

As above, we integrate eq. (3) by parts. However, this time we divide the volume into two parts which are

separated by an internal surface S_1. We obtain

$$\int_V y_i^{(m)}[\rho\omega^2 v_i + (C_{ijkl}v_{k,l})_{,j} + f_i]\,dV - \int_S y_i^{(m)}[(C_{ijkl}v_{k,l})n_j]\,dS - \int_{S_1} y_i^{(m)}[(C_{ijkl}v_{k,l})^+ - (C_{ijkl}v_{k,l})^-]n_j^+\,dS = 0, \quad (m = 1, \ldots, N), \tag{11}$$

where n_j is the outward unit normal vector to the outer surface and n_j^+ is the unit normal to the (arbitrarily chosen) 'upper' surface of S_1, and $(C_{ijkl}v_{k,l})^+$ and $(C_{ijkl}v_{k,l})^-$ are evaluated on the 'upper' and 'lower' surfaces, respectively. Note that the sum of the separate two volume integrals is shown as $\int_V$ in eq. (11).

Considering only the integral on S_1, we find that, as the weight functions $y_i^{(m)}$ are arbitrary, the following natural continuity condition (i.e. continuity of traction) will automatically be satisfied by the weak-form solutions at every point on S_1

$$[(C_{ijkl}v_{k,l})^+ - (C_{ijkl}v_{k,l})^-]n_j^+ = 0. \tag{12}$$

However, as the location of S_1 is arbitrary, continuity of traction will automatically be satisfied by the weak-form solutions everywhere in the medium. The fact that it is not necessary for the trial functions explicitly to satisfy continuity of traction is an important advantage of the weak form, particularly for laterally heterogeneous media.

Some previous workers (e.g. Wiggins 1976; Buland & Gilbert 1984) used the weak form to compute the normal modes of laterally homogeneous media, but used cubic splines as trial and weight functions so that continuity of traction could be explicitly satisfied. Note, however, that the extra effort required to explicitly force the traction to be continuous was unnecessary. Also, this approach cannot be easily generalized to laterally heterogeneous media, for which the effort required to explicitly force the traction to be continuous would be much greater.

2.5 Inhomogeneous boundary conditions

We now consider cases in which the traction or displacement on all or part of the outer boundary is required to be equal to a prescribed value. We obtain the corresponding weak-form operator by adding appropriate boundary integrals to the weak-form operator eq. (9). We consider a medium with a homogeneous boundary condition of the form eq. (8) imposed on a portion of the outer boundary, S_0, an inhomogeneous traction boundary condition of the form

$$(C_{ijkl}v_{k,l})n_j - \tau_i = 0, \quad (i = 1, 2, 3) \tag{13}$$

imposed on a portion of the outer boundary, S_τ, and an inhomogeneous displacement boundary condition of the form

$$v_i - D_i = 0, \quad (i = 1, 2, 3) \tag{14}$$

imposed on the remaining portion of the outer surface S_D. The weak-form operator that satisfies the above boundary conditions is

$$\omega^2\int_V y_i^{(m)}\rho v_i\,dV - \int_V y_{i,j}^{(m)}C_{ijkl}v_{k,l}\,dV + \int_{S_0} y_i^{(m)}S_{ij}v_j\,dS = -\int_V y_i^{(m)}f_i\,dV - \int_{S_\tau} y_i^{(m)}\tau_i\,dS - \int_{S_D} y_{i,j}^{(m)}C_{ijkl}D_k n_l\,dS \quad (m = 1, \ldots, N). \tag{15}$$

Equation (15) is essentially the weak-form version of the representation theorem.

To confirm that the solution of eq. (15) satisfies the boundary conditions on S_0 and S_τ we integrate by parts as follows

$$\int_V y_i^{(m)}[\rho\omega^2 v_i + (C_{ijkl}v_{k,l})_{,j} + f_i]\,dV - \int_{S_0} y_i^{(m)}[(C_{ijkl}v_{k,l})n_j - S_{ij}v_j]\,dS - \int_{S_\tau} y_i^{(m)}[(C_{ijkl}v_{k,l})n_j - \tau_i]\,dS - \int_{S_D} y_i^{(m)}(C_{ijkl}v_{k,l})n_j\,dS + \int_{S_D} y_{i,j}^{(m)}C_{ijkl}D_k n_l\,dS = 0 \quad (m = 1, \ldots, N). \tag{16}$$

As $y_i^{(m)}$ is arbitrary, the natural boundary condition eq. (8) will automatically be satisfied on S_0 by the weak-form solutions obtained from eq. (15). Similarly, we can see that the inhomogeneous boundary condition eq. (13) will be automatically satisfied on S_τ, and that the equation of motion will be satisfied everywhere in V. To confirm that the solution of eq. (15) satisfies eq. (14) on S_D, we integrate eq. (15) by parts as follows:

$$\int_V v_i[\rho\omega^2 y_i^{(m)} + (C_{ijkl}y_{k,l}^{(m)})_{,j}]\,dV + \int_V y_i^{(m)}f_i\,dV - \int_{S_0} v_i C_{ijkl}y_{k,l}^{(m)}n_j\,dS + \int_{S_0} y_i^{(m)}S_{ij}v_j\,dS - \int_{S_\tau} v_i C_{ijkl}y_{k,l}^{(m)}n_j\,dS + \int_{S_\tau} y_i^{(m)}\tau_i\,dS - \int_{S_D} y_{i,j}^{(m)}C_{ijkl}n_l(v_k - D_k)\,dS = 0, \quad (m = 1, \ldots, N). \tag{17}$$

As $y_{i,j}^{(m)}C_{ijkl}n_l$ is arbitrary, we see that $(v_k - D_k)$ must be zero everywhere on S_D. Thus we see that the inhomogeneous boundary conditions eqs (13) and (14) are natural boundary conditions of the augmented operator in eq. (15).

We now consider a dislocation. Suppose S_D^+ is the upper surface of the fault, S_D^- is the lower surface of the fault, and $\Delta_i = v_i^+ - v_i^-$ is the prescribed dislocation. We assume, for simplicitly, that there is no surface with a prescribed traction, so that the surface integral over S_τ can be dropped

from eq. (15), which then becomes

$$\omega^2\int_V y_i^{(m)}\rho v_i\,dV - \int_V y_{i,j}^{(m)}C_{ijkl}v_{k,l}\,dV + \int_{S_0} y_i^{(m)}S_{ij}v_j\,dS$$
$$= -\int_V y_i^{(m)}f_i\,dV + \int_{S_{D+}} y_{i,j}^{(m)}C_{ijkl}\Delta_k n_l\,dS$$
$$(m = 1, \ldots, N). \tag{18}$$

The force, f_i, for which $\int_V y_i^{(m)}f_i\,dV = \int_{S_{D+}} y_{i,j}^{(m)}C_{ijkl}\Delta_k n_l\,dS$ for all $y_i^{(m)}$ is defined to be the equivalent body force. f_i can be obtained from the right-hand side of eq. (18) essentially by inspection

$$f_i(\mathbf{x}) = -\int_{S_{D+}} [\delta(\mathbf{x}-\mathbf{x}_0)]_{,j}C_{ijkl}(\mathbf{x}_0)\Delta_k(\mathbf{x}_0)n_l(\mathbf{x}_0)\,dS(\mathbf{x}_0), \tag{19}$$

where we use $\mathbf{x}_0$ to denote the position on the surface S_{D+}.

The equivalent body force and the dislocation are equivalent in the following sense. We consider two separate solutions of eq. (18). In the first case, we drop the first term on the right-hand side of eq. (18) (i.e. the only inhomogeneous term is due to the dislocation), and in the second case we drop the second term on the right-hand side of eq. (18) and use the value of f_i given by eq. (19) in the first term of eq. (18) (i.e. the only inhomogeneous term is due to the equivalent body force). As the right-hand side of eq. (18) is equal for these two cases, the solutions of eq. (18) (and thus the synthetic seismograms everywhere in the medium) are equal for the two cases. Note that the classic paper by Burridge & Knopoff (1964) proved the equivalence of the body force defined by eq. (19) and the corresponding dislocation using the strong form of the elastic equation of motion. As is well known, eq. (19) can be used to show the equivalence of a shear dislocation and a superposition of double couples for an isotropic medium.

As inhomogeneous displacement or traction boundary conditions can always be replaced by the corresponding equivalent body forces, we will not include the last two terms on the right-hand side of eq. (15) in the results presented in the following sections. However, if desired, these additional inhomogeneous terms can be included in a straightforward manner.

2.6 Partial derivatives

To invert waveform data for earth structure it is necessary to be able to compute the partial derivatives of the synthetic seismograms with respect to changes in the model parameters. To do this we use the first-order Born approximation (e.g. Geller *et al.* 1990a; 1990b; Hara, Tsuboi & Geller 1991). Note that we are not restricted to treating the laterally heterogeneous part of the model as an 'infinitesimal' perturbation to a laterally homogeneous model, as the following results allow us to compute the parital derivatives for a laterally heterogeneous perturbation to a laterally heterogeneous initial model.

We make a perturbation δC_{ijkl} to the elastic moduli and a perturbation $\delta\rho$ to the density. We assume that the coefficients prescribing the natural boundary condition, S_{ij}, remain unchanged. We expand the perturbation to the synthetic seismogram in terms of the trial functions

$$\delta v_i(\mathbf{x}) = \sum_{n=1}^{N} \delta d_n \psi_i^{(n)}(\mathbf{x}). \tag{20}$$

We obtain the weak form of the elastic equation of motion for the perturbed medium from eq. (9). [For simplicity we perturb eq. (9) rather than eq. (15), but the following derivation could equally well be applied to the latter.]

$$\omega^2\int_V y_i^{(m)}(\rho+\delta\rho)(v_i+\delta v_i)\,dV$$
$$-\int_V y_{i,j}^{(m)}(C_{ijkl}+\delta C_{ijkl})(v_{k,l}+\delta v_{k,l})\,dV$$
$$+\int_S y_i^{(m)}S_{ij}(v_j+\delta v_j)\,dS$$
$$= -\int_V y_i^{(m)}f_i\,dV \quad (m = 1, \ldots, N). \tag{21}$$

Note that the unknowns in eq. (21) are the expansion coefficients δd_n in eq. (20). Using eq. (9) and retaining only first-order terms, eq. (21) becomes

$$\omega^2\int_V y_i^{(m)}\rho\,\delta v_i\,dV - \int_V y_{i,j}^{(m)}C_{ijkl}\,\delta v_{k,l}\,dV$$
$$+\int_S y_i^{(m)}S_{ij}\,\delta v_j\,dS$$
$$= -\omega^2\int_V y_i^{(m)}\,\delta\rho\,v_i\,dV + \int_V y_{i,j}^{(m)}\,\delta C_{ijkl}v_{k,l}\,dV$$
$$(m = 1, \ldots, N). \tag{22}$$

Eq. (22) is the weak form of the first-order Born approximation.

2.7 Finite approximation

The preceding discussion assumed that the trial and weight functions were complete sets, but all calculations will be limited to finite bases, which, in general, will not be complete sets. The accuracy and convergence of such finite approximations are discussed in detail by Strang & Fix (1973). Their most important result is Theorem 2.2 (p. 124), which states that in the limit as the basis becomes infinite, and thereby complete, if every element of the strong-form function space can be represented as a superposition of the weak-form trial functions, and if the system of linear equations (eq. 3, eq. 9, or eq. 15) is stably invertible, then the weak-form solution will converge to the strong-form solution. The factors controlling the rate of convergence are discussed by Strang & Fix (1973) and Johnson (1987).

3 FLUID MEDIA

Media containing both fluid and solid regions have posed problems for previous workers using weak-form methods. For example, Wiggins (1976) treated the fluid parts of the medium using the same formulation as for a solid, but setting the rigidity $\mu = 0$. This led to the existence of non-physical modes of vibration due to the extraneous degrees of freedom. Buland & Gilbert (1984, p. 111) used

the same basic approach as Wiggins, but set $\nabla \times \mathbf{u} = \mathbf{0}$ as an additional constraint on the displacement. This approach was apparently not completely successful in suppressing extraneous modes.

In contrast to most previous work, we use (a quantity proportional to) the pressure change as the dependent variable in the fluid regions, and displacement as the dependent variable in the solid regions. Arbitrary numbers of both fluid and solid regions are allowed, and their geometry can also be arbitrary. The continuity conditions at the fluid–solid boundaries are enforced by adding appropriate surface integrals to the weak-form operators for the respective regions. Note that Wu & Rochester (1990) used a somewhat similar approach in their study of core oscillations.

In the remainder of this paper we do not make an explicit distinction between the notation for the strong and weak forms. We use w to denote the weight functions, u to denote the displacement, ϕ to denote the trial functions, and c_n to denote the expansion coefficients of the trial functions. The reader is asked to keep in mind, however, that the weak- and strong-form weight and trial functions belong to different function spaces. We will continue to prove the equivalence of the weak and strong forms through the by now familiar procedure of integrating the weak form by parts.

We begin by considering the case of an isotropic fluid medium. For an isotropic fluid, in which the elastic moduli are equal to $C_{ijkl} = \lambda \delta_{ij} \delta_{kl}$, the strong form of the equation of motion, eq. (2) reduces to

$$\int_V w_i^{(m)} [\rho \omega^2 u_i + (\lambda u_{k,k})_{,i} + f_i] \, dV = 0 \quad (m = 1, \ldots, N). \tag{23}$$

As the weight function $w_i^{(m)}$ is arbitrary, the term in square brackets in eq. (23) must be zero. We solve for u_i:

$$u_i = -\frac{(\lambda u_{k,k})_{,i} + f_i}{\rho \omega^2}. \tag{24}$$

We substitute eq. (24) into the definition of the isotropic component of the stress tensor (i.e. the negative of the pressure change) to obtain

$$P = \lambda u_{k,k} = \lambda \left[\frac{(\lambda u_{k,k})_{,i} + f_i}{-\rho \omega^2} \right]_{,i}. \tag{25}$$

Note that displacement appears in eq. (25) only in the form $\lambda u_{k,k}$. We now define a new scalar variable

$$Q = \frac{P}{\omega} = \frac{\lambda u_{k,k}}{\omega}. \tag{26}$$

We combine eqs (24) and (26) to obtain an expression for the displacement when $f_i = 0$

$$u_i = -\frac{Q_{,i}}{\rho \omega}. \tag{27}$$

We will use eq. (27) in the following when we consider the case of a fluid–solid boundary.

We substitute eq. (26) into eq. (25) to obtain, after a certain amount of manipulation,

$$\frac{\omega^2 Q}{\lambda} + \left[\frac{Q_{,i} + f_i/\omega}{\rho} \right]_{,i} = 0. \tag{28}$$

We have now obtained a scalar equation of motion. We express eq. (28) in MWR form, as

$$\int_V w^{(m)} \left\{ \frac{\omega^2 Q}{\lambda} + \left[\frac{(Q_{,i} + f_i/\omega)}{\rho} \right]_{,i} \right\} dV = 0 \quad (m = 1, \ldots, N), \tag{29}$$

where $w^{(m)}$ is now a *scalar* weight function. Note that eq. (29) is equivalent to eq. (6) of Stephen (1988) when $f_i = 0$.

We represent the solution of eq. (29), Q, as a linear combination of N linearly independent scalar trial functions, $[\phi^{(1)}(\mathbf{x}), \ldots, \phi^{(N)}(\mathbf{x})]$,

$$Q(\mathbf{x}) = \sum_{n=1}^{N} c_n \phi^{(n)}(\mathbf{x}), \tag{30}$$

where the expansion coefficients c_n are the unknowns in eq. (29). At this point in our discussion we assume that the trial functions and weight functions are both complete sets, which may be infinite.

The continuity conditions that must be satisfied by Q are continuity of Q itself, and, in a source-free region, continuity of $Q_{,i} n_i$ in the n_i direction. These conditions must be satisfied by each of the trial functions $\phi^{(n)}(\mathbf{x})$ used in eq. (30).

We now define a weak-form operator which is equivalent to eq. (29)

$$\int_V \left[\frac{\omega^2 w^{(m)} Q}{\lambda} - \frac{w_{,i}^{(m)} (Q_{,i} + f_i/\omega)}{\rho} \right] dV = 0 \quad (m = 1, \ldots, N). \tag{31}$$

In the same way as we obtained eq. (11) from eq. (3), we can, by integrating eq. (31) by parts, show that the continuity of $Q_{,i} n_i$ (which is equivalent to the continuity of the i component of displacement in the $\mathbf{i}$ direction) is a natural continuity condition which will be automatically satisfied by the weak-form solutions without its having to be explicitly satisfied by the trial functions. On the other hand, the continuity of Q (which is equivalent to the continuity of the pressure change) is an essential continuity condition, which must be satisfied by each of the trial functions in eq. (30). The essential and natural continuity conditions for a fluid medium are thus the opposite of those for a solid medium, for which continuity of displacement is an essential continuity condition and continuity of traction is a natural continuity condition.

To demonstrate the equivalence of the strong and weak forms we integrate eq. (31) by parts to obtain

$$\int_V w^{(m)} \left\{ \frac{\omega^2 Q}{\lambda} + \left[\frac{(Q_{,i} + f_i/\omega)}{\rho} \right]_{,i} \right\} dV - \int_S w^{(m)} \left[\frac{(Q_{,i} + f_i/\omega) n_i}{\rho} \right] dS = 0 \quad (m = 1, \ldots, N). \tag{32}$$

The volume integral in eq. (32) is equivalent to the strong form, eq. (29). From the surface integral in eq. (32) we see that the natural boundary condition satisfied by eq. (31) at a force-free boundary is $Q_{,i} n_i = 0$. Eq. (24) shows that this is equivalent to $u_i n_i = 0$ in a source-free region. However, when we consider geophysical problems in media with a fluid region at the outer boundary we usually will want to have a traction-free surface, $Q = 0$. Note that this is an essential boundary condition for eq. (31).

3.1 Fluid–solid medium

We now define a weak-form operator for which the continuity conditions at a fluid–solid boundary are natural continuity conditions. For simplicity, the following discussion assumes that there is no applied body force at the fluid–solid boundary (i.e. $f_i = 0$). The continuity of normal displacement requires

$$\frac{Q_{,i} n_i^{(\mathrm{F})}}{\rho} - \omega u_i n_i^{(\mathrm{S})} = 0, \tag{33}$$

where Q and ρ are evaluated on the fluid side, u_i is the displacement on the solid side, and $n_i^{(\mathrm{F})}$ and $n_i^{(\mathrm{S})}$ are the outward unit normal vectors to the fluid and solid media, respectively. Note that $n_i^{(\mathrm{F})} = -n_i^{(\mathrm{S})}$. Also note that there are no restrictions on the geometry of the fluid–solid boundary.

The continuity of traction requires

$$\omega Q n_i^{(\mathrm{S})} - C_{ijkl} u_{k,l} n_j^{(\mathrm{S})} = 0, \tag{34}$$

where C_{ijkl} are the elastic moduli at the outer boundary of the solid medium, and other quantities are the same as in eq. (33). Note that eq. (34) implies that the tangential tractions at the fluid–solid boundary are zero.

We obtain a weak-form operator that satisfies the fluid–solid boundary conditions eqs (33) and (34) by adding appropriate surface integrals to the weak-form operators eqs (3) and (31)

$$\begin{aligned}
&\omega^2 \int_{V^{(\mathrm{S})}} w_i^{(m)} \rho u_i \, dV - \int_{V^{(\mathrm{S})}} w_{i,j}^{(m)} C_{ijkl} u_{k,l} \, dV \\
&\quad + \int_{S^{(\mathrm{SF})}} \omega w_i^{(m)} Q n_i^{(\mathrm{S})} \, dS = - \int_{V^{(\mathrm{S})}} w_i^{(m)} f_i \, dV \\
&\quad (m = 1, \ldots, NS) \\
&\int_{V^{(\mathrm{F})}} \left[\frac{\omega^2 w^{(m)} Q}{\lambda} - w_{,i}^{(m)} \frac{(Q_{,i} + f_i/\omega)}{\rho} \right] dV \\
&\quad - \int_{S^{(\mathrm{FS})}} \omega w^{(m)} u_i n_i^{(\mathrm{F})} \, dS = 0 \\
&\quad (m = NS + 1, \ldots, NS + NF),
\end{aligned} \tag{35}$$

where $V^{(\mathrm{S})}$ and $V^{(\mathrm{F})}$ are the solid and fluid volumes, respectively, $S^{(\mathrm{SF})}$ is the portion of the outer boundary of the solid medium at the solid–fluid interface, and $S^{(\mathrm{FS})}$ is the portion of the outer boundary of the fluid medium at the solid–fluid interface. NS and NF are the number of trial and weight functions in the solid and fluid media, respectively. The limits of summation in the respective trial function expansions must be appropriately modified. Note that the coupling between the solid and fluid media is accounted for entirely by the two surface integrals in eq. (35).

To demonstrate that eq. (35) satisfies the boundary conditions eqs (33) and (34), we integrate by parts to obtain

$$\begin{aligned}
&\int_{V^{(\mathrm{S})}} w_i^{(m)} [\rho \omega^2 u_i + (C_{ijkl} u_{k,l})_{,j} + f_i] \, dV \\
&\quad - \int_{S^{(\mathrm{SF})}} w_i^{(m)} [(C_{ijkl} u_{k,l}) n_j^{(\mathrm{S})} - \omega Q n_i^{(\mathrm{S})}] \, dS = 0 \\
&\quad (m = 1, \ldots, NS)
\end{aligned} \tag{36}$$

$$\begin{aligned}
&\int_{V^{(\mathrm{F})}} w^{(m)} \left\{ \frac{\omega^2 Q}{\lambda} + \left[\frac{(Q_{,i} + f_i/\omega)}{\rho} \right]_{,i} \right\} dV \\
&\quad - \int_{S^{(\mathrm{FS})}} w^{(m)} \left[\frac{Q_{,i} n_i^{(\mathrm{F})}}{\rho} + \omega u_i n_i^{(\mathrm{F})} \right] dS = 0 \\
&\quad (m = NS + 1, \ldots, NS + NF).
\end{aligned}$$

These results can be generalized to a medium with an arbitrary number of fluid–solid boundaries in a straightforward manner. We do not give the explicit form of the weak-form operator for the partial derivatives, which is obtained following the same general approach as for the solid medium.

The above discussion assumed that the trial and weight functions were complete sets, but all calculations will be limited to finite bases. The discussion of this point in Section 2.7 also applies to the case of fluid–solid media.

4 DIRECT SOLUTION METHOD

We henceforth use the same finite set of functions as both trial functions and weight functions: $w_i^{(m)} = (\phi_i^{(m)})^*$ for a solid, and $w^{(m)} = (\phi^{(m)})^*$ for a fluid. Using the complex conjugates of the trial functions, rather than the trial functions themselves, as the weight functions enhances computational efficiency by minimizing the bandwidth of the linear equations (see Appendix A). The system of linear equations obtained using these weight and trial functions is called the Galerkin weak form of MWR.

We substitute the trial function expansion, eq. (4), into eq. (9) to obtain the Galerkin weak form of the elastic equation of motion for a solid medium with arbitrary natural boundary conditions

$$(\omega^2 \mathbf{T} - \mathbf{H} + \mathbf{R})\mathbf{c} = -\mathbf{g}, \tag{37}$$

where $\mathbf{T}$ is the mass (kinetic energy) matrix, $\mathbf{H}$ is the stiffness (potential energy) matrix, $\mathbf{g}$ is the force vector, and $\mathbf{R}$ is the matrix operator corresponding to the natural boundary condition, eq. (8).

The DSM (Geller *et al.* 1990c) obtains the solution of the weak form of the equation of motion by directly solving the Galerkin weak form of the equation of motion, eq. (37), for a medium with a free surface natural boundary condition (i.e. $\mathbf{R} = 0$). In this paper we extend the DSM to media with arbitrary natural boundary conditions, for which, in general, $\mathbf{R} \neq 0$. We obtain the solution of the weak form of the equation of motion by directly solving eq. (37). In contrast, almost all previous work using the weak form computed synthetic seismograms by modal superposition. We discuss the relation of the DSM to the modal approach in the following.

The explicit form of the matrix elements and vector elements is as follows

$$T_{mn} = \int_V (\phi_i^{(m)})^* \rho \phi_i^{(n)} \, dV \tag{38}$$

$$H_{mn} = \int_V (\phi_{i,j}^{(m)})^* C_{ijkl} \phi_{k,l}^{(n)} \, dV \tag{39}$$

$$R_{mn} = \int_S (\phi_i^{(m)})^* S_{ij} \phi_j^{(n)} \, dS \tag{40}$$

$$g_m = \int_V (\phi_i^{(m)})^* f_i \, dV \tag{41}$$

Note that the subscripts on the left-hand side and the superscripts on the right-hand side of eqs (38) to (41) refer to the abstract vector space of trial functions; the subscripts on the right-hand side of these equations refer to the physical space.

Equation (37) will be singular whenever ω is equal to an eigenfrequency. For a medium with a free surface boundary condition, for which $\mathbf{R}=0$, two cases are of practical importance. If the elastic moduli are real (i.e. if the medium is perfectly elastic), all of the eigenfrequencies will be real, and an imaginary part must be added to ω to ensure that eq. (37) will be non-singular (see Phinney 1965). On the other hand, if the elastic moduli include anelastic attenuation, all of the eigenfrequencies will be complex, and eq. (37) will be non-singular for all real values of ω.

4.1 Partial derivatives of synthetics

The Galerkin form of the first-order Born approximation, eq. (22), is

$$(\omega^2\mathbf{T}-\mathbf{H}+\mathbf{R})\boldsymbol{\delta}\mathbf{c}=-[\omega^2(\boldsymbol{\delta}\mathbf{T})-(\boldsymbol{\delta}\mathbf{H})]\mathbf{c}, \tag{42}$$

where $\mathbf{T}, \mathbf{H}$ and $\mathbf{R}$ are defined in eqs (38), (39) and (40), respectively. The elements of the matrices on the right-hand side of eq. (42) are

$$\delta T_{mn}=\int_V (\phi_i^{(m)})^*\,\delta\rho\phi_i^{(n)}\,dV \tag{43}$$

$$\delta H_{mn}=\int_V (\phi_{i,j}^{(m)})^*\,\delta C_{ijkl}\phi_{k,l}^{(n)}\,dV, \tag{44}$$

where $\delta\rho$ is the perturbation to the density, and δC_{ijkl} is the perturbation to the elastic modulus.

To perform iterative linearized inversion for earth structure, it is not necessary to solve eq. (42) once for each earthquake and each model parameter. Rather we formally write the solution of eq. (42) as

$$\boldsymbol{\delta}\mathbf{c}=-(\omega^2\mathbf{T}-\mathbf{H}+\mathbf{R})^{-1}[\omega^2(\boldsymbol{\delta}\mathbf{T})-(\boldsymbol{\delta}\mathbf{H})]\mathbf{c}, \tag{45}$$

and then, as discussed by Geller & Hara (1993), incorporate eq. (45) into the expressions for the coefficients of the normal equations for the waveform inversion problem.

4.2 Fluid–solid medium

We now present the Galerkin formulation for the fluid–solid medium in eq. (35). For simplicity we assume that the external boundary condition for the solid is a free surface, so we set $\mathbf{R}=0$. We consider a medium with a single solid region and a single fluid region, each of which can be arbitrarily heterogeneous, but the results in the following can be extended to a medium with an arbitrary number of fluid and solid regions (e.g. an ocean over the crust and mantle over the fluid outer core over the solid inner core) in a straightforward way. The Galerkin matrix equation becomes

$$(\omega^2\mathbf{T}-\mathbf{H}+\omega\mathbf{R}')\mathbf{c}=-\mathbf{g}, \tag{46}$$

where $\mathbf{R}'$ is the matrix operator corresponding to the natural continuity conditions (for displacement and normal traction) at the fluid–solid boundary.

The matrix and vector elements for the solid part of the medium are given by eqs (38), (39) and (41). The matrix and vector elements for the fluid and for the fluid–solid boundary are as follows:

$$T_{mn}=\int_V \frac{(\phi^{(m)})^*\phi^{(n)}}{\lambda}\,dV \quad (m>NS,\ n>NS) \tag{47}$$

$$H_{mn}=\int_V \frac{(\phi_{,i}^{(m)})^*\phi_{,i}^{(n)}}{\rho}\,dV \quad (m>NS,\ n>NS) \tag{48}$$

$$g_m=-\int_V \frac{(\phi_{,i}^{(m)})^* f_i}{\rho\omega}\,dV \quad (m>NS) \tag{49}$$

$$R'_{mn}=\int_S (\phi_i^{(m)})^* n_i^{(S)}\phi^{(n)}\,dS \quad (m\leqslant NS,\ n>NS) \tag{50}$$

$$R'_{mn}=\int_S (\phi^{(m)})^* n_i^{(S)}\phi_i^{(n)}\,dS \quad (m>NS,\ n\leqslant NS) \tag{51}$$

$$R'_{mn}=0 \quad (m>NS,\ n>NS) \quad \text{or} \quad (m\leqslant NS,\ n\leqslant NS). \tag{52}$$

Note that in eq. (50) m refers to the vector trial functions for the solid medium and n to the scalar trial functions for the fluid medium, whereas the reverse is true in eq. (51). In general the trial functions can be chosen so that the number of non-zero elements in $\mathbf{R}'$ will be fairly small. Note also that we used $n_i^{(S)}=-n_i^{(F)}$ in eq. (51).

4.3 Relation of DSM to variational method

If the matrix $\mathbf{R}$ and the force vector $\mathbf{g}$ are both equal to zero, (i.e. if the natural boundary conditions are free surface boundary conditions, and if there is no external force) eq. (37) becomes

$$(\omega^2\mathbf{T}-\mathbf{H})\mathbf{c}=0. \tag{53}$$

For a perfectly elastic medium eq. (53) is exactly the same equation obtained when the variational (Rayleigh–Ritz) method is used to formulate the normal-mode problem. The non-trivial solutions of eq. (53) are the expansion coefficients $\mathbf{c}^{(n)}$ for the eigenfunction of the nth mode, when $\omega=\omega_n$ is an eigenfrequency. The normal modes will satisfy a free surface boundary condition unless all of the trial functions satisfy a fixed boundary condition.

If, having solved the normal-mode problem, eq. (53), we then wanted to solve the inhomogeneous problem

$$(\omega^2\mathbf{T}-\mathbf{H})\mathbf{d}=-\mathbf{g} \tag{54}$$

we could expand $\mathbf{d}$ as a linear combination of the orthonormalized eigenfunctions $\mathbf{c}^{(n)}$, where β_n is the excitation coefficient of the nth mode:

$$\mathbf{d}=\sum_n \beta_n\mathbf{c}^{(n)}=\sum_n \left(\frac{[-(\mathbf{c}^{(n)})^*\cdot\mathbf{g}]}{\omega^2-\omega_n^2}\right)\mathbf{c}^{(n)}. \tag{55}$$

We thus can see (as has been pointed out by, for example, Finlayson 1972) that the variational method is merely a special case of the weak form of the equation of motion. However, the variational method can only be applied to media with free or fixed boundary conditions, whereas the weak-form solution can be computed for media with arbitrary natural boundary conditions. Also, the DSM can be applied to anelastic media, although, strictly speaking, the variational method cannot be.

4.4 When should modal superposition be used?

Modal superposition is advantageous when just a few modes are sufficient to represent the physical quantity of interest, as the number of degrees of freedom is thereby greatly reduced. Modal superposition is thus well suited to surface-wave problems, as surface waves can be adequately represented by summing only the contribution of the fundamental and first several higher mode branches. In contrast, modal superposition is not advantageous for the computation of complete synthetic seismograms, as the superposition of all of the modes of the system is required. Modal superposition is also ill-suited to the computation of body-wave synthetics, as an extremely large number of modes must be summed even if the number of modes is reduced by phase-velocity windowing.

There are many instances, such as media with radiation boundary conditions (e.g. Geller *et al.* 1985) for which modes of free oscillation either do not exist, or are not a complete set. Modal superposition methods are inapplicable to such media but many previous workers have used 'locked mode' techniques (Harvey 1981) to compute and superpose the modes of closely related systems. Unfortunately, however, such techniques do not fully eliminate the reflections from the bottom of the medium; they are also unnecessarily computationally intensive. Finally, these techniques are basically limited to the case of a laterally homogeneous medium, although Nolet *et al.* (1989) proposed the use of locked-mode techniques to compute synthetic seismograms for a laterally heterogeneous medium by treating the laterally heterogeneous part of the structure as a small perturbation to the laterally homogeneous model.

It should be noted that hybrid approaches are also possible. For example, Hara *et al.* (1991; 1993) compute synthetic seismograms and partial derivatives for surface waves in a laterally heterogeneous model using the DSM, but they use the eigenfunctions of the degenerate singlets of the fundamental and first few higher toroidal and spheroidal multiplets of the laterally homogeneous model as trial functions, thereby greatly reducing the dimension of the matrices.

4.5 Computational considerations

We now consider the computational requirements for solving eq. (37) (or eq. 46). The standard method for solving systems of simultaneous linear equations consists of two steps. The first step, LU decomposition (with partial pivoting), which requires $O(N^3/3)$ multiplications for a full matrix, is performed only once for each matrix of coefficients. The second step, forward- and back-substitution, which together require only $O(N^2)$ multiplications per solution for a full matrix, is performed once per right-hand side. Usually, however, the trial functions will be chosen so that $(\omega^2\mathbf{T} - \mathbf{H} + \mathbf{R})$ is a banded matrix rather than a full matrix. In this instance the operation counts for the LU factorization and the forward- and back-substitutions are $O[1/2(NB^2)]$ and $O(4NB)$, respectively, where B is the bandwidth (Golub & Van Loan 1989).

We next consider the computational requirements to conduct one iteration of iterative linearized waveform inversion for a single value of the frequency ω (for details see Geller & Hara 1993). The repeated solution of eq. (37) for different right-hand side vectors is the key step in this process. One solution of eq. (37) is required for each earthquake to compute the synthetic seismograms. One solution of eq. (37) is required for each component (Z, east–west, or north–south) of each station to compute the (back-propagated) wavefield generated by a delta-function point force at the station. These wavefields are then used to compute the coefficients and right-hand side of the normal equations for the waveform-inversion problem. Note that only one LU decomposition is required per frequency; all of the other calculations are forward- and back-substitutions which can be performed efficiently.

The explicit forms of the trial functions and matrix elements for several particular examples are discussed in the next section and in the Appendices. We use trial functions whose vertical dependence is expressed by local functions (linear splines), and whose horizontal dependence is expressed by global functions (sines and cosines, Fourier–Bessel expansions, or spherical harmonics for Cartesian, cylindrical and spherical coordinates, respectively). However, if desired, these results could also be used for purely local trial functions or purely global trial functions.

5 NUMERICAL EXAMPLES

5.1 Laterally homogeneous case

We first consider the laterally homogeneous 2-D Cartesian medium shown in Fig. 1, for which the source is a line source. We solve the equation of motion for a series of discrete frequencies and wavenumbers, $\omega_n = 2\pi n/T$ and $(k_x)_n = 2\pi n/L$, where T is the duration of the seismograms and L is the length of the domain in the x-direction. We then compute the inverse Fourier transform from the (ω, k_x, z) domain to the (t, x, z) domain using the Fast Fourier Transform (FFT).

To compute the inverse Fourier transform with respect to the wavenumber k_x, we have to ensure that there are no poles along the real k_x-axis. The examples given in the following do not include anelastic attenuation. We therefore, following Phinney (1965), introduce a small imaginary part into the frequency of the form $\omega = \omega_R - i\omega_I$. The effect of this artificial damping is then removed from the final time history by multiplying by $\exp(\omega_I t)$. Because both ω and k_x are sampled at discrete points, aliasing in both time and space (in the horizontal direction) is a problem, but the aliasing is ameliorated by the artificial damping.

Figure 2 shows the results of a simple test calculations. For simplicity, and because we verified our results by comparing them with analytical results, we show the results for a homogeneous medium. However, note that no additional computational effort would be required for an arbitrarily vertically heterogeneous medium. The snapshots in the right-hand column of Fig. 2 show that there are no reflections from the lower boundary when a radiation boundary is imposed. In contrast, the left-hand column of Fig. 2 shows that artificial reflections from the lower boundary heavily contaminate the wavefield when a free surface boundary condition is used.

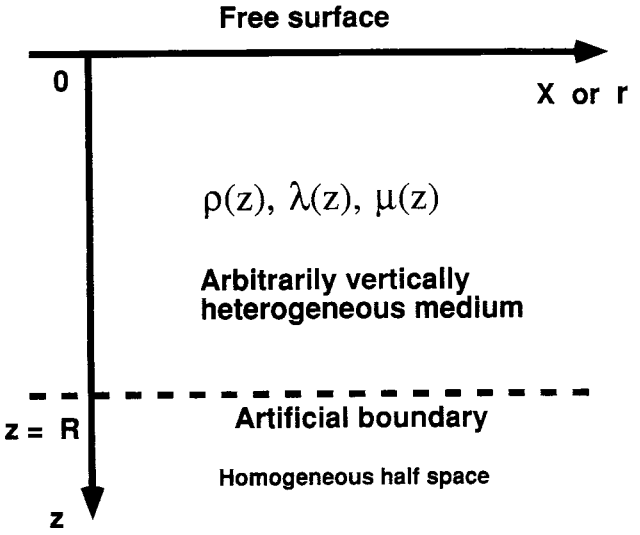

Figure 1. Parameters for laterally homogeneous, isotropic model. The density, ρ, and elastic constants, λ and μ, are functions of depth only. We place an artificial boundary at depth $z = R$. The horizontal coordinate is 'x' for 2-D problems in Cartesian coordinates and 'r' for 3-D problems in cylindrical coordinates, respectively.

Next we present results for P–SV wave propagation in a homogeneous medium, using a point source (a downward point force) and cylindrical coordinates. The inverse transformation from the (ω, k_r, z) domain to the (t, r, z) domain is performed in essentially the same way as for the Cartesian P–SV case, except that the inverse spatial transform is a Bessel transform rather than a Fourier transform. Note that the synthetics computed using our method include both body-wave and surface-wave contributions. Figs 3(a) and (b) show a series of snapshots for the wavefield excited by a point source at the left edge of the figure at a depth of 3 km. In addition to the direct and reflected P and SV waves, Rayleigh waves can be seen moving along the surface. Note the decay of the Rayleigh wave ampltiude with depth. Also note that the radiation condition at the lower boundary is fully effective in suppressing artificial reflections. The above numerical results are all for cartesian or cylindrical coordinates. Recently, Cummins *et al.* (1993) used the DSM to compute synthetics for SH (toroidal) displacement for laterally homogenous media and spherical coordinates.

5.2 2-D basin models

We consider SH wave propagation in the 2-D laterally and vertically heterogeneous medium shown in Fig. 4. We represent the (SH) tangential displacement using trial functions whose horizontal dependence is of the form $\exp(-il\pi x/L)$, but whose vertical dependence is given by locally defined linear splines $W_p(z)$ (Fig. 5)

$$u_y(x, z) = \sum_{l=-N_L/2+1}^{N_L/2} \sum_{p=1}^{N_p} c_{lp} W_p(z) \exp(-il\pi x/L). \qquad (56)$$

Note that there are two subscripts on the expansion coefficients, as they depend on both l and p. We introduce more general notation for the trial functions and expansion coefficients in Appendix A.

We impose a radiation boundary condition at the bottom of the region (see Appendix B for details). For the side boundaries, we use a method proposed by Smith (1974). The initial artificial reflection is eliminated by adding together the solution of the Dirichlet (fixed) and Neumann (free) problems. We use sines (Dirichlet problem) and cosines (Neumann problem), rather than exponentials, as the horizontally dependent part of the trial functions. As is well known, Smith's method eliminates the initial artificial reflections from the side boundaries, but does not eliminate reflections which encounter the same face more than once. As we use a radiation boundary condition at the lower boundary, multiple reflections will occur only between the two side boundaries or near the upper corners. However, the distance between the two side boundaries or near the upper corners. However, the distance between the two side boundaries is sufficiently large that contamination by such higher order reflections does not pose a serious problem. Future work should consider various other possibilities for the artificial boundary condition at the side boundaries.

To check the validity of our method, we compare our numerical results with those obtained using other techniques. We consider SH waves in the basin structure of Fig. 6, which has already been studied by various methods. For example, Kohketsu (1987a,b) calculated synthetic seismograms for this model using the generalized reflectivity method, which is essentially the Aki & Larner (1970) technique extended to multilayered media. We use a Ricker wavelet (Fig. 7) as the source-time function. We compare our method (DSM), generalized reflectivity (RF) (Kohketsu 1987a) and the FEM (Fig. 8). The FEM seismograms were computed by D. Suetsugu (private communication). Our results (DSM) and the RF synthetic seismograms are in good agreement. The later portion of the FEM synthetic seismograms are contaminated by artificial reflections, as an absorbing boundary condition was not used. However, except for these artificial reflections, the FEM synthetic seismograms agree well with the RF and DSM results.

We next consider the basin model shown in Fig. 9. Fig. 10 shows synthetic seismograms computed for a plane-wave incident from below. Amplification due to focusing caused by the laterally heterogeneous structure can be clearly observed. Calculations of this type have the potential to contribute to an understanding of the strong ground motion in sedimentary basins (e.g. Sánchez-Sesma *et al.* 1988).

5.3 Truncation of coupling matrix

The trial functions in eq. (56) can be used for an arbitrarily laterally heterogeneous model, but they are particularly well suited to cases for which the laterally heterogeneous earth structure is relatively smooth. For such cases, the seismic wavefield can be approximated by considering only coupling between nearby wavenumbers, and truncating the full matrix of coupling coefficients to omit coupling between more distant wavenumbers.

We now investigate the degradation in accuracy due to truncating the matrices (i.e. setting the matrix elements for coupling between distant wavenumbers to zero). Fig. 11 shows the effect of such truncation on the waveforms. For each receiver, the top trace is the correct result, and the bottom trace is computed ignoring all coupling between wavenumbers. The middle three traces show the results for the partially truncated cases. We divide the group of N_L

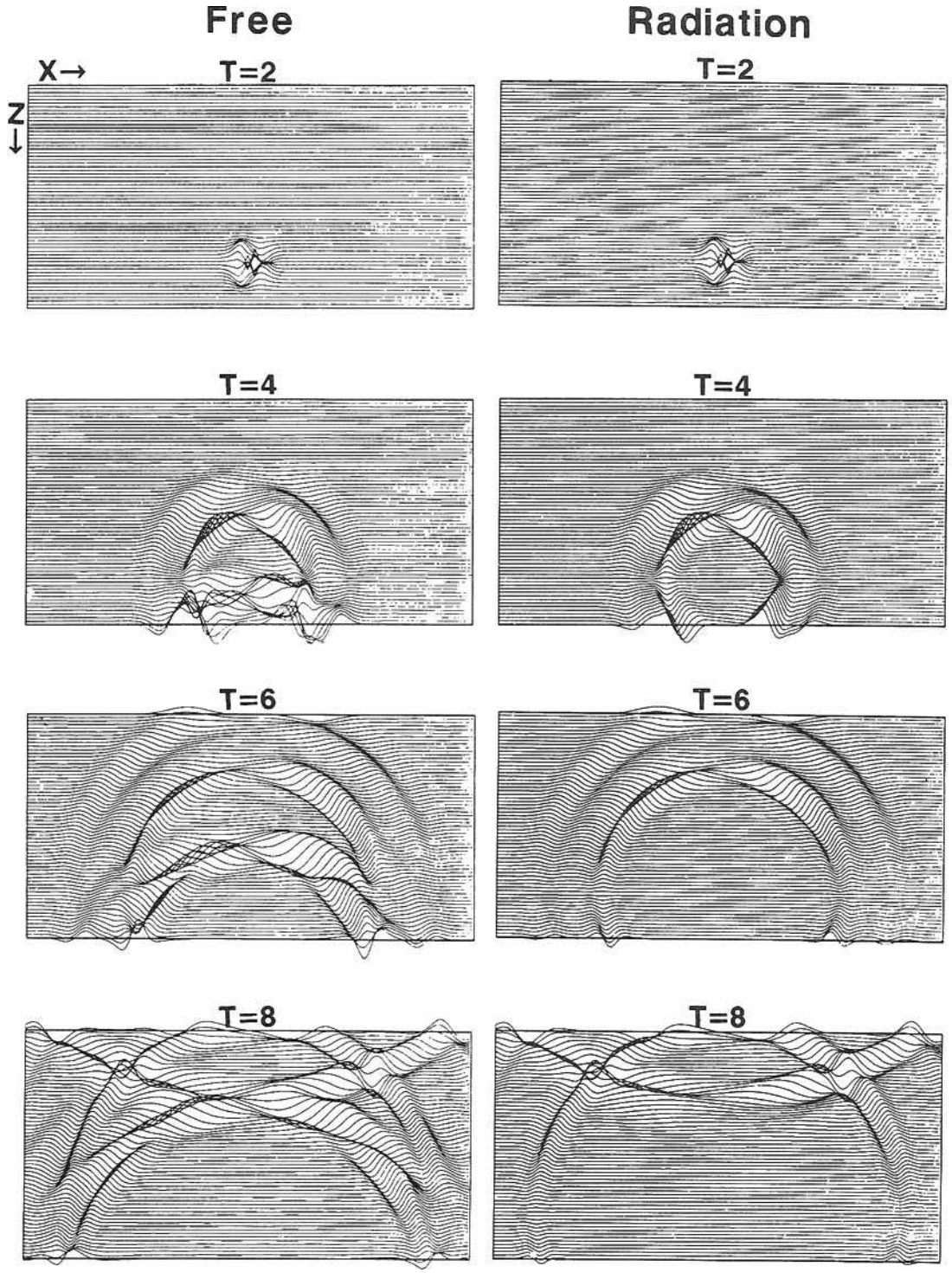

Figure 2. Snapshots of *P–SV*-wave propagation for a line source. The medium is homogeneous and isotropic with $\alpha = 5.0\,\mathrm{km\,s^{-1}}$ and $\beta = 3.5\,\mathrm{km\,s^{-1}}$. The top boundary is a free surface. We impose a radiation boundary condition at the bottom boundary for the snapshots on the right, but a free lower boundary is used for the left-hand snapshots. Note that the left-hand snapshots are heavily contaminated by artificial reflections from the lower boundary for $T \geqslant 4\,\mathrm{s}$. The calculation is for a 2-D (plane strain) case. The source is a downward force (line source) The x-component of displacement is shown in both sets of snapshots.

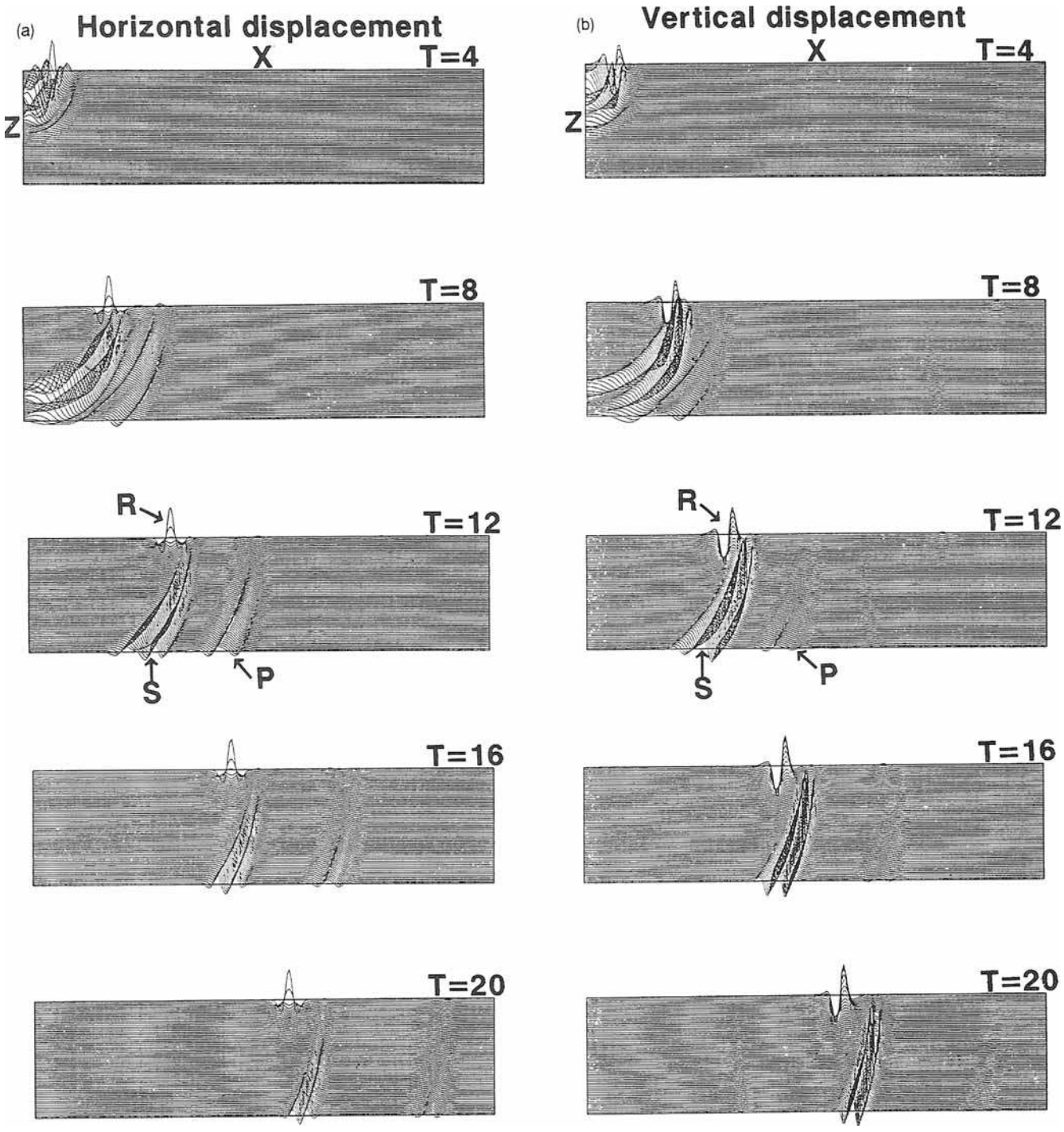

Figure 3. (a) Snapshots of waves from a point source in a homogeneous half-space with $\alpha = 5.0\,\mathrm{km\,s^{-1}}$ and $\beta = 3.5\,\mathrm{km\,s^{-1}}$. A downward single force is applied at depth $z = 3.0\,\mathrm{km}$ at the left edge of the figure. In addition to P and SV waves, the Rayleigh wave can also be seen. The radiation boundary condition is fully effective in eliminating artificial reflections from the lower boundary. The horizontal component of displacement is shown. (b) Same as (a), but the vertical component of displacement is shown.

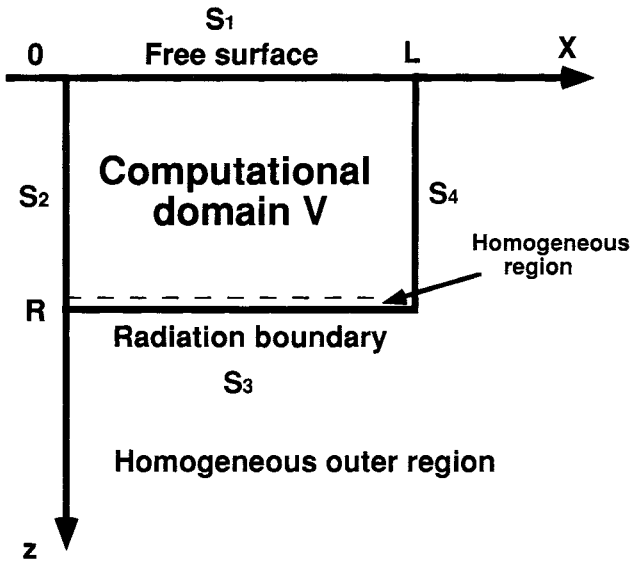

Figure 4. Computational domain V for the 2-D, quasi-arbitrarily heterogeneous case. The upper boundary S_1 is a free surface; S_2, S_3 and S_4 are artificial boundaries. We use Smith's method to eliminate the initial reflections from the side boundaries S_2 and S_4. We impose a radiation condition on the lower boundary S_3. The medium must be homogeneous and isotropic in an infinitesimally thin zone above the radiation boundary, but can otherwise be arbitrarily heterogeneous.

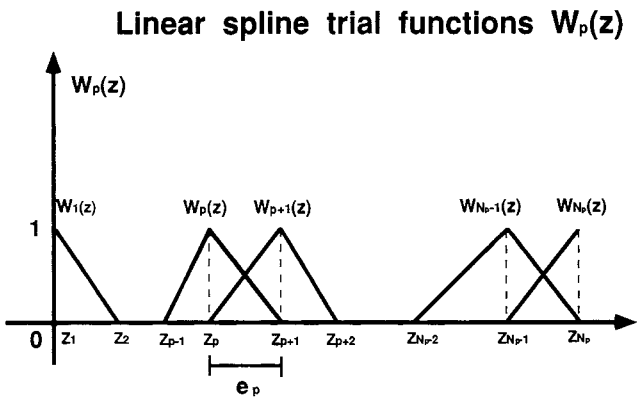

Figure 5. Locally defined linear spline functions, $W_1(z), \ldots, W_{N_p}(z)$. The displacement field from $z = 0$ to $z = R$ is represented as a linear combination of the N_p spline functions. Only $W_p(z)$ and $W_{p+1}(z)$ are non-zero in the pth element. Note that there are N_p trial functions, but only $N_p - 1$ elements.

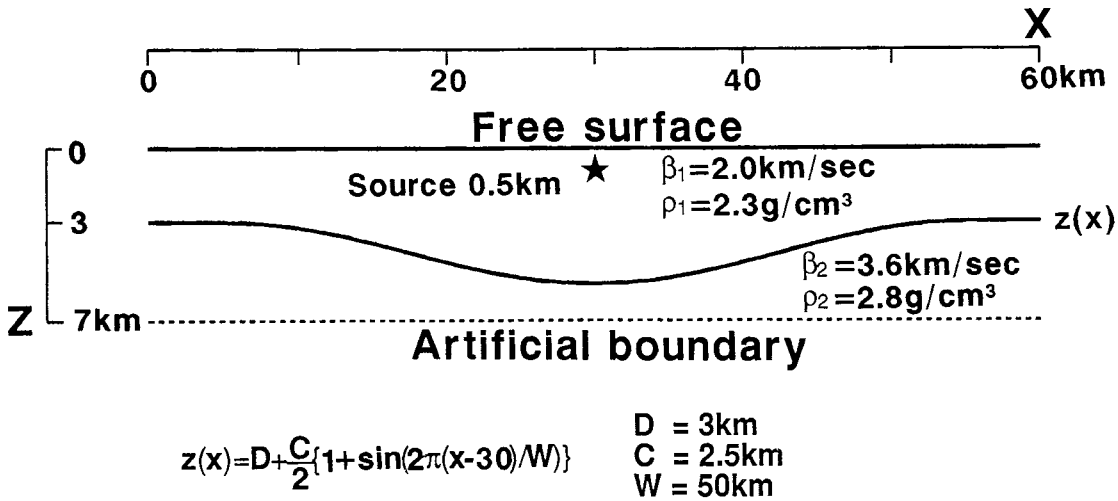

Figure 6. Basin model for the 2-D laterally heterogeneous *SH* calculation. A line source is buried in the centre of the basin at a depth of 0.5 km. The artificial lower boundary is located at a depth of 7 km. The elastic properties are as shown. The equation at the bottom gives the shape of the bottom of the basin.

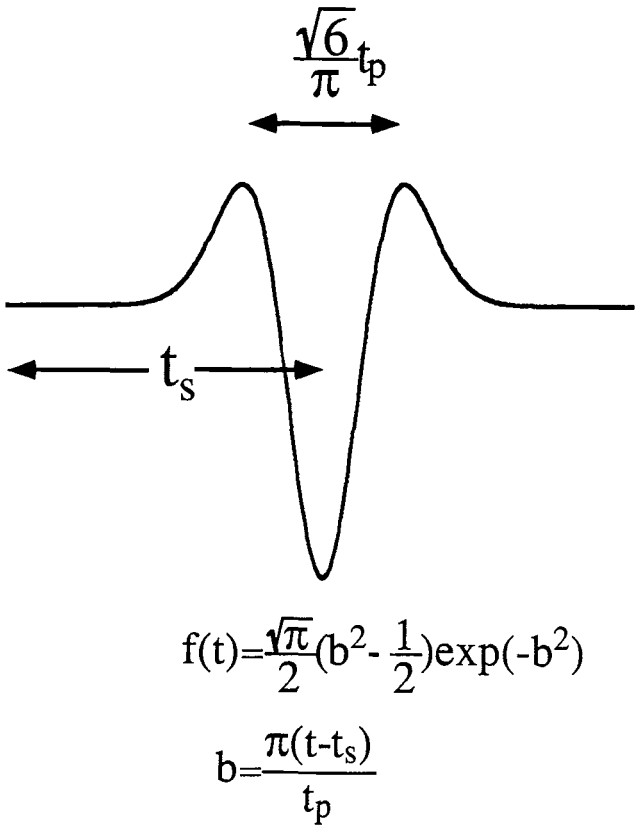

Figure 7. Ricker wavelet used as a source-time function throughout this paper.

wavenumbers into two groups of $N_L/2$, four groups of $N_L/4$, and eight groups of $N_L/8$, and truncate all intergroup coupling. The synthetic seismograms appear almost unchanged for the $N_L/2$ case. For the $N_L/4$ case, the trace at epicentral distance $\Delta = 0$ km is slightly distorted, but the other traces are almost unchanged. For the $N_L/8$ case there is more distortion, but the error is still not so large. Thus the $N_L/4$ case seems to be an acceptable approximation to the exact solution, but the $N_L/8$ results seem marginal. Determining the optimum trade-off between accuracy and CPU time is an important topic for future research.

6 DISCUSSION

We have presented all of the basic results necessary to compute synthetic seismograms and their partial derivatives by using the DSM to solve the weak form of the elastic equation of motion. These results have the potential to be useful in future work on analysing seismic waveforms to determine earth structure and earthquake-source processes.

Probably the reason weak-form methods have not previously been used more extensively is that strong-form methods have been able to handle satisfactorily almost all of the computations necessary for laterally homogeneous media in cylindrical or Cartesian coordinates. As these methods are well known and software is widely available, there has been no need to consider using weak-form methods. In contrast, future work in seismology will concentrate much more on laterally heterogeneous media, and laterally homogeneous media with spherical coordinates (i.e. whole-earth calculations that do not use earth

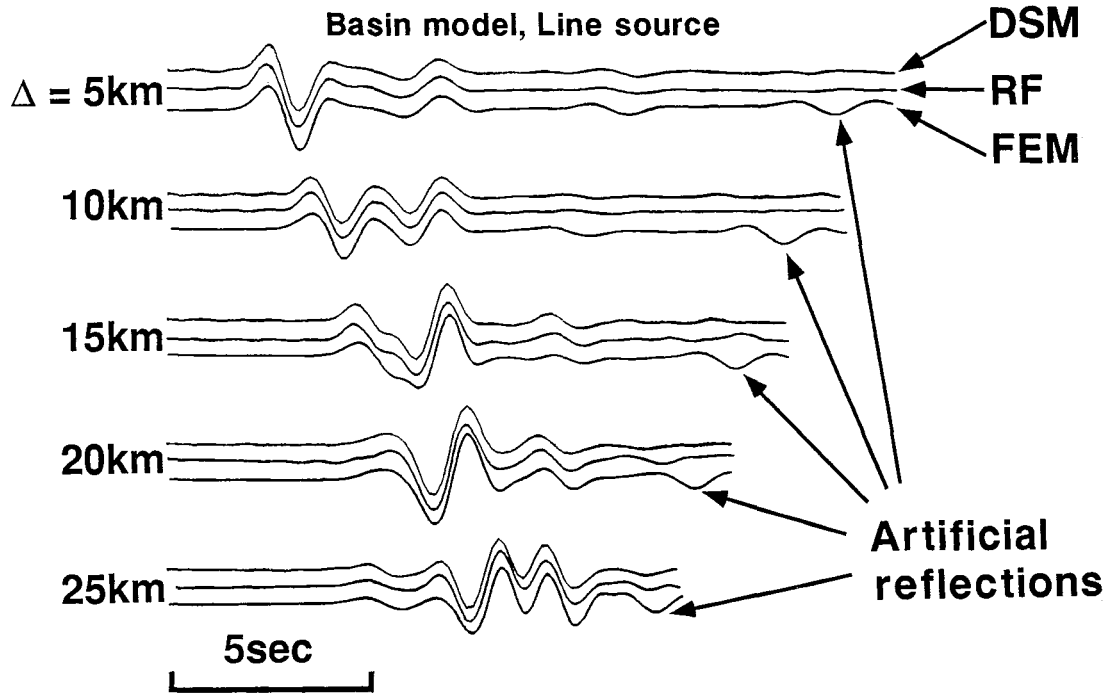

Figure 8. Comparison of synthetic seismograms for three methods for the basin model in Fig. 6. The direct solution method (DSM), generalized reflectivity (RF) method and ordinary finite-element method (FEM) are used. The traces are the tangential component of displacement at distances of 5, 10, 15, 20 and 25 km from the centre of the basin, where a line source is buried at 0.5 km depth. For each epicentral distance, results from the three methods are compared (top, DSM; middle, RF; and bottom, FEM) All three methods agree excellently, except for the artificial reflections in the later part of the FEM results, which occur because a radiation boundary condition was not used.

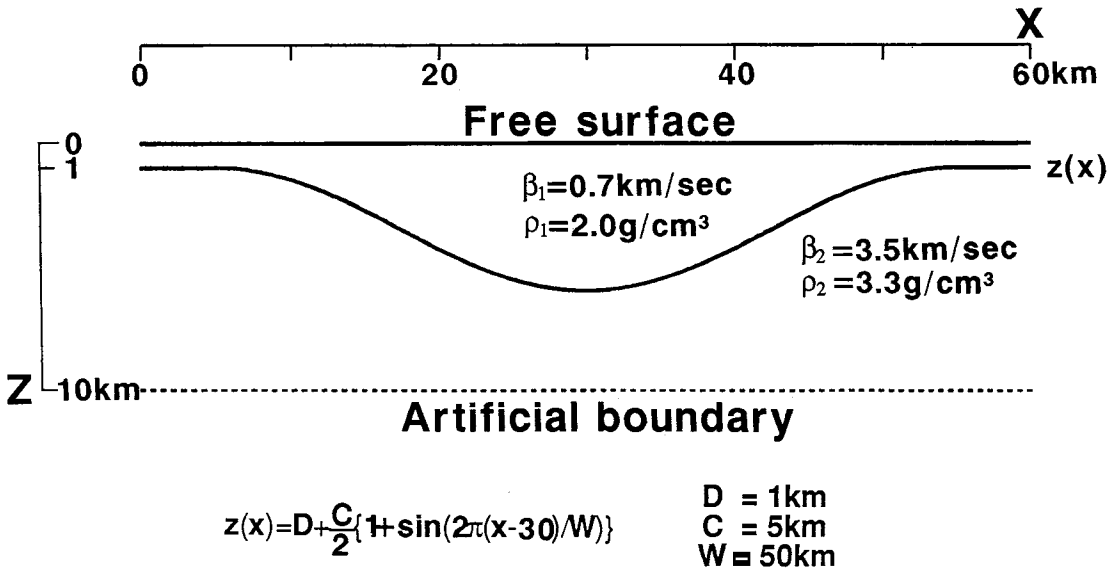

Figure 9. 2-D basin structure with a soft sediment layer. A plane *SH* wave is impinging vertically from the lower half-space. Note that this model differs from the model used in Fig. 6.

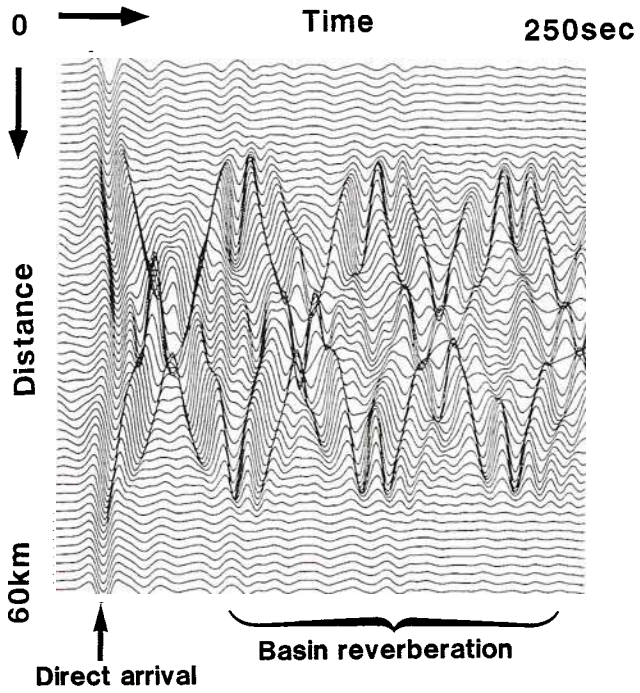

Figure 10. Amplification of incident waves by the basin structure shown in Fig. 9. A plane *SH* wave is vertically incident from below. Amplification due to constructive interference is clearly visible in the centre of the basin.

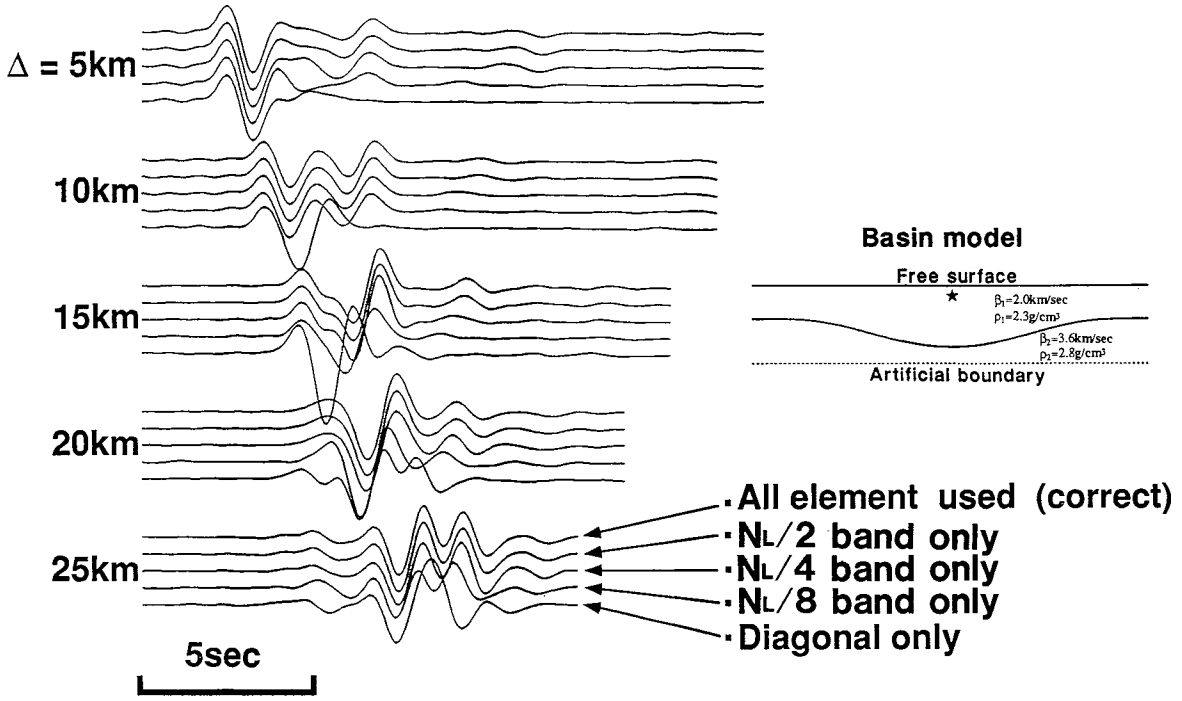

Figure 11. Effect of truncating the coupling between wavenumbers for the model shown in Fig. 6. The blocks in the untruncated block tridiagonal matrix each have dimension $N_L \times N_L$. At each epicentral distance, traces correspond to, from top to bottom: (1) the exact solution; (2) $N_L/2$ band only; (3) $N_L/4$ band only; (4) $N_L/8$ band only; and (5) diagonal terms only. From top to bottom the accuracy decreases, but the computational efficiency increases. In the basin model, $\beta_1 = 2.0\,\mathrm{km\,s^{-1}}$ and $\rho_1 = 2.3\,\mathrm{g\,cm^{-3}}$ in the upper layer; in the lower layer, $\beta_2 = 3.6\,\mathrm{km\,s^{-1}}$ and $\rho_2 = 2.8\,\mathrm{g\,cm^{-3}}$.

flattening approximations). It seems likely that weak-form methods can make useful contributions to the solution of such problems.

ACKNOWLEDGMENTS

We thank Kazuki Kohketsu for advice and for allowing us to use some of his software. We thank Daisuke Suetsugu for advice and for calculating the FEM synthetics shown in Fig. 8. We benefited greatly from many discussions with Tatsuhiko Hara, Phil Cummins and Naoki Kobayashi. We also thank Phil Cummins for critically reading several versions of the manuscript and suggesting many significant improvements.

We used HITAC S-820/80, HITAC M-680H and VAX8600 computer systems at the Computer Center of Tokyo University. This research was partially supported by a grant from the Japanese Ministry of Education, Science and Culture (No. 05640463). This research was carried out under the ISM Cooperative Research Program (93-ISM · CRP-57).

REFERENCES

Aki, K. & Larner, K. L., 1970. Surface motion of a layered medium having an irregular interface due to incident plane *SH* waves, *J. geophys. Res.*, **75,** 933–954.

Alekseev, A. S. & Mikhailenko, B. G., 1976. The solution of Lamb's problem for a vertically inhomogeneous elastic half-space, *Izv. Earth Phys. (Engl. Trans.)*, **12,** 748–755.

Alekseev, A. S. & Mikhailenko, B. G. 1980. The solution of dynamic problems of elastic wave propagation in inhomogeneous media by a combination of partial separation of variables and finite-difference method, *J. Geophys.*, **48,** 161–172.

Boore, D. M., 1970. Love waves in nonuniform wave guides: finite difference calculations, *J. geophys. Res.*, **75,** 1512–1527.

Bouchon, M., 1981. A simple method to calculate Green's functions for elastic layered media, *Bull. seism. Soc. Am.*, **71,** 959–971.

Bouchon, M. & Aki, K., 1977a. Discrete wave-number representation of seismic source wave fields, *Bull. seism. Soc. Am.*, **67,** 259–277.

Bouchon, M. & Aki, K., 1977b. Near-field of a seismic source in a layered medium with irregular interfaces, *Geophys. J. R. astr. soc.*, **50,** 669–684.

Buland, R. & Gilbert, F., 1984. Computation of free oscillations of the Earth, *J. comput. Phys.*, **54,** 95–114.

Burridge, R. & Knopoff, L., 1964. Body force equivalents for seismic dislocations, *Bull. seism. Soc. Am.*, **54,** 1875–1888.

Cerjan, C., Kosloff, D., Kosloff, R. & Reshef, M., 1985. A nonreflecting boundary condition for discrete acoustic and elastic wave equations, *Geophysics*, **50,** 705–708.

Červený, V., 1983. Synthetic body wave seismograms for laterally varying layered structures by the Gaussian beam method, *Geophys. J. R. astr. Soc.*, **73,** 389–426.

Chang, W. F. & McMechan, G. A., 1989. Absorbing boundary conditions for 3-D acoustic and elastic finite-difference calculations, *Bull. seism. Soc. Am.*, **79,** 211–218.

Chapman, C. H. & Orcutt, J. A., 1985. The computation of body wave synthetic seismograms in laterally heterogeneous media, *Rev. Geophys.*, **23,** 105–163.

Clayton, R. & Engquist, B., 1977. Absorbing boundary conditions for acoustic and elastic wave equation, *Bull. seism. Soc. Am.*, **67,** 1529–1549.

Courant, R., 1943. Variational methods for the solution of problems of equilibrium and vibrations, *Bull. Am. Math. Soc.*, **49,** 1–23.

Cummins, P. R., Geller, R. J., Takeuchi, N. & Hatori, T., 1993. DSM complete synthetic seismograms I: *SH*, spherically symmetric case, *Geophys. Res. Lett.*, submitted.

Dautray, R. & Lions, J.-L., 1988. *Mathematical Analysis and Numerical Methods for Science and Technology,* 6 Vols, Springer-Verlag, Berlin.

Engquist, B. & Majda, A., 1977. Absorbing boundary conditions for the numerical simulation of waves, *Math. Comput.*, **31,** 629–651.

Engquist, B. & Majda, A., 1979. Radiation boundary conditions for acoustic and elastic wave calculations, *Commun. Pure appl. Math.*, **32,** 313–357.

Finlayson, B. A., 1972. *The Method of Weighted Residuals and Variational Principles,* Academic Press, New York.

Fix, G. J. & Marin, S. P., 1978. Variational method for underwater acoustic problems, *J. comput. Phys.*, **28,** 253–270.

Fletcher, C. A. J., 1984, *Computational Galerkin Method,* Springer-Verlag, New York.

Fuchs, K. & Müller, G., 1971. Computation of synthetic seismograms with the reflectivity method and comparison with observations, *Geophys. J. R. astr. Soc.* **23,** 417–433.

Geller, R. J. & Hara, T. 1993. Two efficient algorithms for iterative linearized inversion of seismic waveform data, *Geophys. J. Int.*, **115,** 699–710.

Geller, R. J., Hara, T. & Tsuboi, S., 1990a. On the equivalence of two methods for computing partial derivatives of seismic waveforms, *Geophys. J. Int.*, **100,** 153–156.

Geller, R. J., Hara, T. & Tsuboi, S., 1990b. On the equivalence of two methods for computing partial derivatives of seismic waveforms—II. Laterally homogeneous initial model, *Geophys. J. Int.*, **102,** 499–502.

Geller, R. J., Hara, T., Tsuboi, S. & Ohminato, T., 1990c. A new algorithm for waveform inversion using a laterally heterogeneous starting model, in *Seismological Society of Japan Fall Meeting,* 296 [in Japanese].

Geller, R. J., Noack, R. M. & Fetter, A. L., 1985. Normal mode solutions for absorbing boundary conditions, *Geophys. Res. Lett.*, **12,** 145–148.

Goldstine, C. I., 1982. A finite element method for solving Helmholtz type equations in waveguides and other unbounded domains, *Math. Comput.*, **39,** 309–324.

Golub, G. & Van Loan, C. F., 1989. *Matrix Computations,* 2nd edn, Johns Hopkins, Baltimore.

Hara, T., Tsuboi, S. & Geller, R. J., 1991. Inversion for laterally heterogeneous earth structure using a laterally heterogeneous starting model: preliminary results, *Geophys. J. Int.*, **104,** 523–540.

Hara, T., Tsuboi, S. & Geller, R. J. 1993. Inversion for laterally heterogeneous upper mantle *S*-wave velocity structure using iterative waveform inversion, *Geophys. J. Int.*, **115,** 667–698.

Harvey, D. J., 1981. Seismogram synthesis using normal mode superposition: the locked mode approximation, *Geophys. J. R. astr. Soc.*, **66,** 37–69.

Haskell, N. A., 1953. The dispersion of surface waves in multi-layered media, *Bull. seism. Soc. Am.*, **43,** 17–43.

Higdon, R. L., 1990. Radiation boundary conditions for elastic wave propagation, *SIAM J. Numer. Anal.*, **27,** 831–870.

Johnson, C., 1987. *Numerical Solution of Partial Differential Equations by the Finite Element Method,* Cambridge University Press, Cambridge.

Jones, M. N., 1985. *Spherical Harmonics and Tensors for Classical Field Theory,* Research Studies Press, Letchworth.

Kausel, E., 1992. Physical interpretation and stability of paraxial boundary conditions, *Bull. seism. Soc. Am.*, **82,** 898–913.

Kelly, K. R., Ward, R. W., Treitel, S. & Alford, R. M., 1976. Synthetic seismograms: a finite difference approach, *Geophysics,* **41,** 2–26.

Kennett, B. L. N., 1983. *Seismic Wave Propagation in Stratified Media,* Cambridge University Press, Cambridge.

Kohketsu, K., 1987a. 2-D Reflectivity method and synthetic seismograms in irregularly layered structures. I. *SH*-wave generation, *Geophys. J. R. astr. Soc.*, **89,** 821–838.

Kohketsu, K., 1987b. Synthetic seismograms in realistic media: a wave theoretical approach, *Bull. Earthq. Res. Inst., Univ. Tokyo,* **62,** 201–245.

Korn, M., 1987. Computation of wavefields in vertically inhomogeneous media by a frequency domain finite difference method and application to wave propagation in earth models with random velocity and density perturbations, *Geophys. J. R. astr. Soc.*, **88,** 345–377.

Kosloff, D. & Baysal, E., 1982. Forward modeling by a Fourier method, *Geophysics,* **47,** 1402–1412.

Lindmann, E. L., 1975. Free-space boundary conditions for the time dependent wave equation, *J. comput. Phys.*, **18,** 66–78.

Liu, H.-P., Anderson, D. L. & Kanamori, H., 1976. Velocity dispersion due to anelasticity: implications for seismology and mantle composition, *Geophys. J. R. astr. Soc.*, **47,** 41–58.

Lysmer, J. & Drake, L. A., 1972. *A finite element method for seismology, Meth. in comput. phys.*, **11,** 181–216.

Lysmer, J. & Kuhlemeyer, R. L., 1969. Finite dynamic model for infinite media, *J. Eng. Mech. Div., ASCE,* **95,** 859–877.

Marfurt, K. J., 1984. Accuracy of finite-difference and finite-element modeling of the scalar and elastic wave equations, *Geophysics,* **49,** 533–549.

Mikhailenko, B. G., 1985. Numerical experiment in seismic investigations, *J. geophys.*, **58,** 101–124.

Nolet, G., Sleeman, R., Nijhof, V. & Kennett, B. L. N., 1989. Synthetic reflection seismograms in three dimensions by a locked mode approximation, *Geophysics,* **54,** 350–358.

Olson, A. H., Orcutt, J. A. & Frazier, G. A., 1984. The discrete wavenumber/finite element method for synthetic seismograms, *Geophys. J. R. astr. Soc.*, **77,** 421–460.

Phinney, R. A., 1965. Theoretical calculation of the spectrum of first arrivals in layered elastic mediums, *J. geophys. Res.*, **70,** 5107–5123.

Phinney, R. A. & Burridge, R., 1973. Representation of the elastic-gravitational excitation of a spherical earth model by generalized spherical harmonics, *Geophys. J. R. astr. Soc.*, **34,** 451–487.

Randall, C. J., 1988. Absorbing boundary conditions for the elastic wave equation, *Geophysics,* **53,** 611–624.

Reynolds, A. C., 1978. Boundary conditions for the numerical solution of wave propagation problems, *Geophysics,* **43,** 1099–1110.

Sánchez-Sesma, F., Chávez-Peñez, S., Suárez, M., Bravo, M. A. & Pérez-Rocha, L. E., 1988. The Mexico Earthquake of September 19, 1985—on the seismic response of the valley of Mexico, *Earthq. Spectra,* **4,** 569–589.

Smith, W. D., 1974. A non-reflecting plane boundary for wave propagation problems, *J. comput. Phys.*, **15,** 492–503.

Smith, W. D., 1975. The application of finite element analysis to body wave propagation problems, *Geophys. J. R. astr. Soc.* **42,** 747–768.

Spudich, P. & Ascher, U., 1983. Calculation of complete theoretical seismograms in vertically varying media using collocation methods, *Geophys. J. R. astr. Soc.*, **75,** 101–124.

Stephen, R. A., 1988. A review of finite difference methods for seismo-acoustics problems at the seafloor, *Rev. Geophys.*, **26,** 445–458.

Strang, G. & Fix, G. J., 1973. *An Analysis of the Finite Element Method,* Prentice Hall, Englewood Cliffs, NJ.

Takeuchi, H. & Saito, M., 1972. Seismic surface waves, *Meth. comput. Phys.*, **11,** 217–295.

Thomson, W. T., 1950. Transmission of elastic waves through a stratified solid, *J. appl. Phys.*, **21,** 89–93.

Wiggins, R. A., 1976. A fast, new computational algorithm for free oscillations and surface waves, *Geophys. J. R. astr. Soc.*, **47,** 135–150.

Wu, W.-J. & Rochester, M. G., 1990. Core dynamics: the two-potential description and a new variational principle, *Geophys. J. Int.*, **103,** 697–706.

APPENDIX A: TRIAL FUNCTIONS AND MATRIX ELEMENTS

In this Appendix we consider only a solid medium, but the same general procedures apply to a fluid or a fluid–solid medium. The DSM obtains the expansion coefficients of the trial functions by solving eq. (37), the Galerkin weak form of the equation of motion

$$(\omega^2\mathbf{T} - \mathbf{H} + \mathbf{R})\mathbf{c} = -\mathbf{g}, \tag{A1}$$

where $\mathbf{T}$ is the mass matrix, $\mathbf{H}$ is the stiffness matrix, $\mathbf{R}$ is the matrix corresponding to the natural boundary condition, and $\mathbf{g}$ is the vector of excitation coefficients. To minimize the CPU time required to solve eq. (A1), we minimize the bandwidth of the matrices on the left-hand side of eq. (A1), and, to the extent possible, break up eq. (A1) into a series of smaller uncoupled systems of linear equations. Minimizing the bandwidth of eq. (A1) and decomposing eq. (A1) into decoupled systems of linear equations depends on the matrix elements and excitation coefficients, which in turn depend on the choice of trial functions, the elastic properties of the medium, and the type and location of the source.

A1 Trial functions

We use trial functions which are the product of local functions of depth (linear splines) and global functions of the horizontal coordinates (Fourier, Fourier–Bessel, or spherical harmonic expansions for Cartesian, cylindrical or spherical coordinates, respectively). Such trial functions are well suited to media in which the vertical heterogeneity is more pronounced than the lateral heterogeneity. The use of purely global or purely local trial functions is also possible, but we do not consider such trial functions in this Appendix.

Four indices are necessary to specify the trial function: p identifies the vertical dependence of the trial functions (see Fig. 5), l and m give the horizontal dependence of the trial functions (e.g. the angular order and azimuthal order of spherical harmonics), and n identifies the polarization of the trial functions (e.g. which of the three vector spherical harmonics is specified).

In this Appendix we denote the trial functions by $\phi_i^{(\alpha)}$ ($\alpha = 1, \ldots, \alpha_{\max}$) rather than $\phi_i^{(n)}$. α can be viewed as a pointer to a mapping table, in which the four indices $\{p_\alpha, l_\alpha, m_\alpha, n_\alpha\}$ that characterize the αth trial function are listed. The order of the entries $\{p_\alpha, l_\alpha, m_\alpha, n_\alpha\}$ is chosen so that the bandwidth of each of the uncoupled systems of linear equations is minimized.

The linear splines $W_p(z)(p = 1, \ldots, N_p)$ specify the vertical dependence of the trial functions

$$W_p(z) = \begin{cases} \dfrac{z - z_{p-1}}{z_p - z_{p-1}}, & z \in [z_{p-1}, z_p] \\ \dfrac{z_{p+1} - z}{z_{p+1} - z_p}, & z \in [z_p, z_{p+1}] \\ 0 & \text{(elsewhere)} \end{cases} . \tag{A2}$$

The first line of eq. (A2) is ignored for $p = 1$ and the second line is ignored for $p = N_p$.

In Cartesian (x, y, z) coordinates, the vector trial functions are

$$\begin{aligned} \mathbf{S}^1(x, y, z) &= W_p(z)(0, 0, Y_{lm}) \quad (n = 1) \\ \mathbf{S}^2(x, y, z) &= W_p(z)(Y_{lm}, 0, 0) \quad (n = 2) \\ \mathbf{S}^3(x, y, z) &= W_p(z)(0, Y_{lm}, 0) \quad (n = 3) \end{aligned} \tag{A3}$$

where

$$Y_{lm}(x, y) = N_{lm} \exp(-il\Delta k_x x) \exp(-im\Delta k_y y),$$
$$(l, m = 0, \pm 1, \pm 2, \ldots)$$

$$\Delta k_x = \frac{2\pi}{L_x}, \qquad \Delta k_y = \frac{2\pi}{L_y},$$

L_x and L_y are the length of the computational domain (where $0 \leq x \leq L_x$ and $0 \leq y \leq L_y$), and N_{lm} is a normalization constant.

For a cylindrical (r, ϕ, z) coordinate system, the vector trial functions are

$$\begin{aligned} \mathbf{S}^1(r, \phi, z) &= W_p(z)(0, 0, Y_{lm}) \quad (n = 1) \\ \mathbf{S}^2(r, \phi, z) &= W_p(z)\left(\frac{1}{k_l}\frac{\partial Y_{lm}}{\partial r}, \frac{1}{rk_l}\frac{\partial Y_{lm}}{\partial \phi}, 0\right) \quad (n = 2) \\ \mathbf{S}^3(r, \phi, z) &= W_p(z)\left(\frac{1}{rk_l}\frac{\partial Y_{lm}}{\partial \phi}, -\frac{1}{k_l}\frac{\partial Y_{lm}}{\partial r}, 0\right) \quad (n = 3) \end{aligned} \tag{A4}$$

where

$$Y_{lm}(r, \phi) = N_{lm} J_m(k_l r) \exp(im\phi),$$
$$(l = 0, 1, 2, \ldots, \text{and } m = 0, \pm 1, \pm 2, \ldots),$$

where J_m is an mth order Bessel function, k_l is the lth wavenumber, and N_{lm} is a normalization constant. The values of k_l depend on the choice of discretization. If we use the algorithm of Bouchon (1981), $k_l = 2\pi l/L$, where L is the radial distance between the evenly spaced concentric sources.

For a spherical (θ, ϕ, r) coordinate system, the trial functions are

$$\begin{aligned} \mathbf{S}^1(\theta, \phi, r) &= W_p(r)(0, 0, Y_{lm}) \quad (n = 1) \\ \mathbf{S}^2(\theta, \phi, r) &= W_p(r)\left(\frac{\partial Y_{lm}}{\partial \theta}, \frac{1}{\sin\theta}\frac{\partial Y_{lm}}{\partial \phi}, 0\right) \quad (n = 2) \\ \mathbf{S}^2(\theta, \phi, r) &= W_p(r)\left(-\frac{1}{\sin\theta}\frac{\partial Y_{lm}}{\partial \phi}, \frac{\partial Y_{lm}}{\partial \theta}, 0\right) \quad (n = 3) \end{aligned} \tag{A5}$$

where

$$Y_{lm}(\theta, \phi) = (-1)^m N_l^m P_l^m(\cos\theta) \exp(im\phi),$$
$$l = 0, 1, 2, \ldots \text{ and } 0 \leq m \leq l$$

$$Y_{lm}(\theta, \phi) = Y^*_{l-m}(\theta, \phi) \qquad l = 1, 2, \ldots \text{ and } -l \leq m < 0,$$

$P_l^m(\cos\theta)$ is an associated Legendre function, and N_l^m is the normalization factor. Note that for cylindrical and spherical coordinates $n=1$ and $n=2$ correspond to the spheroidal displacement, and $n=3$ corresponds to toroidal displacement. This is true for the Cartesian case only when the wavenumber vector lies in the x–z plane.

A2 Matrix elements and selection rules

The matrix elements are given by eqs (38), (39) and (40), and the vector of excitation coefficients is given by eq. (41). We repeat these equations below, but we use α' and α in place of m and n as the indices for the trial functions. α' is a pointer to the indices $\{p_{\alpha'}, l_{\alpha'}, m_{\alpha'}, n_{\alpha'}\}$ that characterize the α'th trial function and α is a pointer to the indices $\{p_\alpha, l_\alpha, m_\alpha, n_\alpha\}$ that characterize the αth trial function.

$$T_{\alpha'\alpha}=\int_V (\phi_i^{(\alpha')})^* \rho \phi_i^{(\alpha)}\, dV \tag{A6}$$

$$H_{\alpha'\alpha}=\int_V (\phi_{i,j}^{(\alpha')})^* C_{ijkl} \phi_{k,l}^{(\alpha)}\, dV \tag{A7}$$

$$R_{\alpha'\alpha}=\int_S (\phi_i^{(\alpha')})^* S_{ij} \phi_j^{(\alpha)}\, dS \tag{A8}$$

$$g_{\alpha'}=\int_V (\phi_i^{(\alpha')})^* f_i\, dV. \tag{A9}$$

For cylindrical or spherical coordinates the derivatives with respect to the l-coordinate, $\phi_{k,l}^{(\alpha)}$, in eq. (A7) are the locally Cartesian derivatives for the respective curvilinear coordinate system.

Using $\{p_\alpha, l_\alpha, m_\alpha, n_\alpha\}$ to denote the indices pointed to by α allows $\{p_\alpha, l_\alpha, m_\alpha, n_\alpha\}$ to be unambiguously identified as belonging to the αth trial function, but this notation is cumbersome. In the remainder of this Appendix we simplify the notation by dropping the subscripts; we use $\{p, l, m, n\}$ to denote the indices for the α-th trial function, and $\{p', l', m', n'\}$ to denote the indices for the α'th trial function. l is used both as one of the four indices $\{p, l, m, n\}$ that characterize the αth trial function, and as one of the dummy subscripts of the elastic modulus C_{ijkl} in eq. (A7), but it should be clear from the context which usage of l is intended.

Integrals of the type in eqs (A6) and (A7) were first considered extensively in quantum mechanics, but such integrals have also been considered widely in seismology (e.g. Phinney & Burridge 1973), fluid dynamics and other branches of classical physics (e.g. Jones 1985), and there is a well-developed set of techniques for their evaluation. The same basic techniques used to evaluate the volume integrals in eqs (A6) and (A7) can also be used to evaluate the surface integral in eq. (A8). The evaluation of the excitation coefficients given by eq. (A9) is discussed in the next section.

To evaluate the integrals in eqs (A6) and (A7) we transform them to the general form

$$\sum \int dz[\cdots] \int dS[\cdots], \tag{A10}$$

where we use z here as a generic variable that represents the vertical coordinate in Cartesian, cylindrical, or spherical coordinates. (Note that in Cartesian or cylindrical coordinates z is positive in the downward direction, but the opposite is true for spherical coordinates.) Similarly we use dS here as a generic variable that represents the area of an infinitesimal horizontal element in Cartesian, cylindrical, or spherical coordinates. The discussion for the remainder of this Appendix is restricted to the case of spherical coordinates, except where otherwise noted. However, the following discussion can be modified to apply to cylindrical or Cartesian coordinates with relatively minor changes, such as replacing 'generalized spherical harmonics' by the corresponding functions for cylindrical or Cartesian coordinates, and 'angular order' and 'azimuthal order' by the corresponding indices for cylindrical or cartesian coordinates.

The summation in eq. (A10) arises from expanding the elastic moduli and density in terms of generalized spherical harmonics, and then summing over all the harmonics for which the integrals are non-zero (see, for example, Jones 1985). The integrals in the summation in eq. (A10) will be zero unless certain selection rules are satisfied. The selection rules depend on the indices characterizing the trial functions, $\alpha' \rightarrow \{p', l', m', n'\}$ and $\alpha \rightarrow \{p, l, m, n\}$. For example, each of the $\int dz[\cdots]$ terms will contain products of functionals of the p'th and pth splines. We can see from eq. (A2) that these products, and, therefore, $\int dz[\cdots]$, will be zero unless $|p'-p| \leqslant 1$. The selection rules governing $\int dS[\cdots]$ depend on the earth model and on the horizontal dependence and polarization of the α'th and αth trial functions, which are indicated by $\{l', m', n'\}$ and $\{l, m, n\}$, respectively. The evaluation of such surface integrals for the case of a general laterally heterogeneous, anisotropic medium in spherical coordinates is discussed by, for example, Jones (1985, Chapter 9); similar results can be derived for cylindrical or Cartesian coordinates.

The evaluation of the integrals that the selection rules show to be non-zero can be performed in a straightforward fashion. The $[\cdots]$ term in $\int dz[\cdots]$ is a low-order polynomial that can be integrated analytically. The $\int dS[\cdots]$ can be evaluated either through the use of the Clebsch–Gordan series for generalized spherical harmonics (or the equivalent for cylindrical or Cartesian coordinates) or numerical quadrature. We do not give explicit results here.

A2.1 Selection rules: laterally homogeneous case

We now consider the case of a laterally homogeneous isotropic (or transversely isotropic) medium. This paragraph considers only cylindrical or spherical coordinates, except where the Cartesian case is mentioned parenthetically. It is well known (e.g. Phinney & Burridge 1973, Jones 1985) that each of the $\int dS[\cdots]$ in eq. (A10) will be zero unless $l=l'$ and $m=m'$. We therefore can break up eq. (A1) into separate equations for each angular order l and azimuthal order m (i.e. we can perform separation of variables). Furthermore, it is well known that the value of $\int dS[\cdots]$ in eq. (A10) depends only on the angular order, l, and not on the azimuthal order, m. Therefore the coefficients in the decoupled systems of linear equations that we obtain from eq. (A1) need be computed only once per angular order, regardless of the number of azimuthal orders that we

consider for that angular order. (Because of the way Y_{lm} is defined earlier for Cartesian coordinates, $\int dS[\cdots]$ depends only on l^2+m^2, but not on the individual values of l and m.) Finally, it is well known that $\int dS[\cdots]$ is zero if $n=3$ and $n'=(1 \text{ or } 2)$, or if $n=(1 \text{ or } 2)$ and $n'=3$. Thus, after decomposing eq. (A1) into separate linear systems for each l and m, we can further decompose these systems into two separate systems of linear equations, one for the toroidal case ($n=n'=3$) and one for the spheroidal case ($n=1$ or 2 and $n'=1$ or 2). Because of the selection rules for the splines, $|p'-p| \leqslant 1$, each of these systems of linear equations will be block tridiagonal. The dimension of the blocks is 1×1 for the toroidal system ($n=3$ only) and 2×2 for the spheroidal system ($n=1$ and $n=2$).

A2.2 Selection rules: laterally heterogeneous case

Trial functions of different angular orders ($l \neq l'$) and different azimuthal orders ($m \neq m'$) are coupled (have non-zero matrix elements) for a laterally heterogeneous medium. By expanding the 3-D structure in generalized spherical harmonics (or the corresponding functions for cylindrical or Cartesian coordinates), the matrix elements can be calculated in a straightforward fashion (see Phinney & Burridge 1973, or Jones 1985). However, as there is a limit to the size of the systems of linear equations that can be solved by any given computer, truncation (setting to zero the matrix elements for coupling between trial functions whose angular orders—wavenumbers, if we are considering cylindrical or Cartesian coordinates—differ by more than a certain amount) of the matrices in eq. (A1) is unavoidable for 3-D laterally heterogeneous problems, in view of the maximum memory capacity of present supercomputers. In contrast, 2-D laterally heterogeneous problems, such as those considered in Sections 5.2 and 5.3, can sometimes be solved without truncating the matrices. We obtain a series of uncoupled block-tridiagonal systems of linear equations as a result of the truncation (see the example in Section 5.3). Each of the systems of uncoupled linear equations obtained from eq. (A1) by truncating the coupling is block tridiagonal, because of the selection rule $|p'-p| \leqslant 1$. The dimension of each block is equal to the number of coupled trial functions.

A3 Excitation coefficients

For both laterally homogeneous media and laterally heterogeneous media the excitation coefficients, given by eq. (A9), will in general be non-zero for all values of the indices l and m. However, for spherical or cylindrical coordinates the number of non-zero excitation coefficients can be drastically reduced by placing the source on the z-axis. For a point force on the z-axis only the $|m| \leqslant 1$ excitation coefficients are non-zero, and for a point moment tensor on the z axis only the $|m| \leqslant 2$ excitation coefficients are non-zero (e.g. Takeuchi & Saito 1972). It is thus highly advantageous to place the source on the z-axis for a laterally homogeneous medium, because only the decoupled matrices for $|m| \leqslant 2$ (for a point moment tensor) or $|m| \leqslant 1$ (for a point force) need be considered.

On the other hand, there is no special advantage to placing the source on the z axis in a laterally heterogeneous medium, as all of the different angular orders and azimuthal orders are coupled by the matrix on the left-hand side of eq. (A1). Thus, even if only a small number of the excitation coefficients are non-zero (as is the case for a point source on the z axis), the expansion coefficients of the trial functions for the solution of eq. (A1) will in general be non-zero for all azimuthal orders for a laterally heterogeneous medium.

A4 Mapping tables

We now present some examples of the mapping tables that relate α to the indices p, l, m and n that characterize the αth vector trial function. We begin by presenting an example of the mapping tables for toroidal (SH) displacement for an isotropic laterally homogeneous medium with spherical coordinates (Table A1). We assume we are considering a case with a point source on the z axis, so that only the case of $-2 \leqslant m \leqslant 2$ need be considered, except that $-1 \leqslant m \leqslant 1$ for $l=1$. Note that $l=0$ need not be considered, as there is no toroidal displacement. All of the mapping tables for laterally homogeneous media that are presented in the following could, if desired, be easily be extended to run from $-l \leqslant m \leqslant l$ rather than from $-2 \leqslant m \leqslant 2$ for sources not on the z axis.

The horizontal double lines in Table A1 separate the various decoupled problems, i.e. the various systems of linear equations that can each be solved separately. As discussed earlier the decoupling is the result of the selection rules for the matrix elements. The large braces on the right-hand side indicate that the matrix elements are the same for each of the decoupled systems of linear equations enclosed by the braces, because the matrix elements depend only on l and not on m. Thus only the vector of excitation coefficients, $\mathbf{g}$, will be different for each of the systems enclosed by the braces. Note that for a point moment tensor on the z axis the excitation coefficients for toroidal displacement will be zero for $m=0$, so this case could be omitted from the mapping table if desired.

Table A1 shows that each trial function corresponds to a unique value of α. However, for simplicity, it is convenient to number the trial functions for each decoupled problem (separated by the double horizontal lines in Table A1) starting from $\alpha=1$. We therefore renumber the trial functions as shown in Table A2. Strictly speaking we should introduce one more index to identify the decoupled problem, so that we could unambiguously discuss $\alpha=1$ for the first decoupled problem, the second decoupled problem, etc. However, the problem under discussion will usually be clear from the context, so we do not explicitly introduce a fifth index (see Table A2). Note that Tables A1 and A2 are identical as far as their content and meaning; only the numbering scheme for α is different.

The mapping table for spheroidal displacement in a laterally homogeneous isotropic (or transversely isotropic) medium with spherical coordinates is given in Table A3. Note that the displacement for $l=0$ is purely radial ($n=1$), but that the displacement for $l \geqslant 1$ includes both vertical ($n=1$) and horizontal ($n=2$) components. As shown in Table A3, we arrange the trial functions so that the vertical and horizontal trial functions for the same value of p, the index for the spline functions that specify the vertical dependence, are grouped together. Choosing any other

order would lead to a larger bandwidth for the decoupled systems of linear equations (although the number of non-zero elements would not change), and thus would increase the CPU time needed to solve the decoupled systems of linear equations.

Tables A4 and A5 show the mapping tables for the 2-D *SH* case (Cartesian coordinates) discussed in Sections 5.2 and 5.3. Note that the index m is omitted in both of these tables, because the problem is 2-D. Table A4 shows the mapping table for the complete problem, and Table A5 shows the mapping table for the truncated problem for which numerical results are given in Fig. 11. In both Tables A4 and A5 a single horizontal line is used to separate trial functions with different values of the index p. The braces on the right of the tables indicate each system of linear equations; note that this convention is different from the meaning of the braces in Tables A1–A3.

By comparing Tables A4 and A5 it can be seen that in both cases we arrange the ordering so that all of the trial functions with the same value of p (i.e. the same linear spline function) are grouped together. In this way we ensure that the matrices in both the original and truncated versions of eq. (A1) will be block tridiagonal. Each of the two truncated matrices in Table A5 fortuitously has the

Table A1. Mapping table for the laterally homogeneous isotropic toroidal (*SH*) case in spherical coordinates.

α	p	l	m	n	
1	1	1	-1	3	
2	2	1	-1	3	
3	3	1	-1	3	
⋮	⋮	⋮	⋮	⋮	
N_p	N_p	1	-1	3	
N_p+1	1	1	0	3	
N_p+2	2	1	0	3	
N_p+3	3	1	0	3	
⋮	⋮	⋮	⋮	⋮	
$2N_p$	N_p	1	0	3	
$2N_p+1$	1	1	1	3	
$2N_p+2$	2	1	1	3	
$2N_p+3$	3	1	1	3	
⋮	⋮	⋮	⋮	⋮	
$3N_p$	N_p	1	1	3	$l=1$
$3N_p+1$	1	2	-2	3	
$3N_p+2$	2	2	-2	3	
$3N_p+3$	3	2	-2	3	
⋮	⋮	⋮	⋮	⋮	
$4N_p$	N_p	2	-2	3	
⋮	⋮	⋮	⋮	⋮	$l=2$
$7N_p+1$	1	2	2	3	
$7N_p+2$	2	2	2	3	
$7N_p+3$	3	2	2	3	
⋮	⋮	⋮	⋮	⋮	
$8N_p$	N_p	2	2	3	
⋮	⋮	⋮	⋮	⋮	$l=\cdots$

Table A2. Mapping table for the laterally homogeneous isotropic toroidal (*SH*) case in spherical coordinates. Same as Table A1, but the trial functions for each decoupled problem are numbered starting from $\alpha=1$.

α	p	l	m	n	
1	1	1	-1	3	
2	2	1	-1	3	
3	3	1	-1	3	
⋮	⋮	⋮	⋮	⋮	
N_p	N_p	1	-1	3	
N_p+1	1	1	0	3	
N_p+2	2	1	0	3	
N_p+3	3	1	0	3	
⋮	⋮	⋮	⋮	⋮	
$2N_p$	N_p	1	0	3	
$2N_p+1$	1	1	1	3	
$2N_p+2$	2	1	1	3	
$2N_p+3$	3	1	1	3	
⋮	⋮	⋮	⋮	⋮	
$3N_p$	N_p	1	1	3	$l=1$
$3N_p+1$	1	2	-2	3	
$3N_p+2$	2	2	-2	3	
$3N_p+3$	3	2	-2	3	
⋮	⋮	⋮	⋮	⋮	
$4N_p$	N_p	2	-2	3	
⋮	⋮	⋮	⋮	⋮	$l=2$
$7N_p+1$	1	2	2	3	
$7N_p+2$	2	2	2	3	
$7N_p+3$	3	2	2	3	
⋮	⋮	⋮	⋮	⋮	
$8N_p$	N_p	2	2	3	
⋮	⋮	⋮	⋮	⋮	$l=\cdots$

Table A3. Mapping table for the laterally homogeneous isotropic spheroidal (P–SV) case in spherical coordinates. Numbering scheme for α follows Table A2.

α	p	l	m	n	
1	1	0	0	1	$l = 0$
2	2	0	0	1	
⋮	⋮	⋮	⋮	⋮	
N_p	N_p	0	0	1	
1	1	1	-1	1	$l = 1$
2	1	1	-1	2	
3	2	1	-1	1	
4	2	1	-1	2	
⋮	⋮	⋮	⋮	⋮	
$2N_p$ -1	N_p	1	-1	1	
$2N_p$	N_p	1	-1	2	
⋮	⋮	⋮	⋮	⋮	
1	1	1	1	1	
2	1	1	1	2	
⋮	⋮	⋮	⋮	⋮	
$2N_p$ -1	N_p	1	1	1	
$2N_p$	N_p	1	1	2	
1	1	2	-2	1	$l = 2$
2	1	2	-2	2	
⋮	⋮	⋮	⋮	⋮	
$2N_p$ -1	N_p	2	-2	1	
$2N_p$	N_p	2	-2	2	
⋮	⋮	⋮	⋮	⋮	
1	1	2	2	1	
2	1	2	2	2	
⋮	⋮	⋮	⋮	⋮	
⋮	⋮	⋮	⋮	⋮	$l = \cdots$

dimension $N_pN_L/2$, but there is no general requirement that truncation must lead to decoupled matrices of equal dimensions. For example, Hara *et al.* (1991; 1993) used the eigenfunctions of degenerate multiplets of the modes of free oscillation of a laterally homogeneous model as their trial functions; their decoupled systems of linear equations were not all of equal dimension.

APPENDIX B: RADIATION BOUNDARY CONDITION

In this Appendix we present examples of media for which a radiation boundary condition at the lower boundary can be

Table A4. Mapping table for the 2-D laterally heterogeneous (SH) case in Cartesian coordinates.

α	p	l	n	
1	1	$-N_L/2+1$	3	$-N_L/2 < l \leq N_L/2$
2	1	$-N_L/2+2$	3	
3	1	$-N_L/2+3$	3	
⋮	⋮	⋮	⋮	
N_L	1	$N_L/2$	3	
N_L+1	2	$-N_L/2+1$	3	
N_L+2	2	$-N_L/2+2$	3	
N_L+3	2	$-N_L/2+3$	3	
⋮	⋮	⋮	⋮	
$2N_L$	2	$N_L/2$	3	
⋮	⋮	⋮	⋮	
$(N_p-1)N_L+1$	N_p	$-N_L/2+1$	3	
$(N_p-1)N_L+2$	N_p	$-N_L/2+2$	3	
$(N_p-1)N_L+3$	N_p	$-N_L/2+3$	3	
⋮	⋮	⋮	⋮	
N_pN_L	N_p	$N_L/2$	3	

Table A5. Mapping table for 2-D laterally heterogeneous (SH) case in Cartesian coordinates when the coupling is truncated to obtain two decoupled problems.

α	p	l	n	
1	1	$-N_L/2+1$	3	$l \leq -N_L/4$ or $l > N_L/4$
2	1	$-N_L/2+2$	3	
⋮	⋮	⋮	⋮	
$N_L/4$	1	$-N_L/4$	3	
$N_L/4+1$	1	$N_L/4+1$	3	
⋮	⋮	⋮	⋮	
$N_L/2$	1	$N_L/2$	3	
$N_L/2+1$	2	$-N_L/2+1$	3	
⋮	⋮	⋮	⋮	
$3N_L/4$	2	$-N_L/4$	3	
$3N_L/4+1$	2	$N_L/4+1$	3	
⋮	⋮	⋮	⋮	
N_L	2	$N_L/2$	3	
⋮	⋮	⋮	⋮	
$(N_p-1)N_L/2+1$	N_p	$-N_L/2+1$	3	
⋮	⋮	⋮	⋮	
$(2N_p-1)N_L/4$	N_p	$-N_L/4$	3	
$(2N_p-1)N_L/4+1$	N_p	$N_L/4+1$	3	
⋮	⋮	⋮	⋮	
$N_pN_L/2$	N_p	$N_L/2$	3	
1	1	$-N_L/4+1$	3	$-N_L/4 < l \leq N_L/4$
2	1	$-N_L/4+2$	3	
⋮	⋮	⋮	⋮	
$N_L/2$	1	$N_L/4$	3	
$N_L/2+1$	2	$-N_L/4+1$	3	
⋮	⋮	⋮	⋮	
N_L	2	$N_L/4$	3	
⋮	⋮	⋮	⋮	
$(N_p-1)N_L/2+1$	N_p	$-N_L/4+1$	3	
⋮	⋮	⋮	⋮	
$N_pN_L/2$	N_p	$N_L/4$	3	

specified in the form of natural boundary conditions (e.g. eq. 8). The solution obtained from the augmented weak-form operator (e.g. eq. 9) will therefore automatically satisfy the radiation boundary condition, as it is a natural boundary condition. The media considered in this Appendix can be arbitrarily heterogeneous in general, but a thin strip just above the lower boundary must be homogeneous and isotropic (Fig. 4).

We present results in this Appendix for three cases of 2-D media with Cartesian coordinates: (1) *SH* waves in a laterally homogeneous medium; (2) *P–SV* waves in a laterally homogeneous medium; and (3) *SH* waves in a laterally heterogeneous medium. The following derivations, with only minor changes, can also be applied to media with cylindrical coordinates, but explicit results are not given here. Radiation boundary conditions are usually unnecessary for media with spherical coordinates, as the exponential decay of amplitude below the turning depth serves much the same purpose; however, radiation boundary conditions can be formulated if desired.

B1 Laterally homogeneous media

Because separation of variables applies to the laterally homogeneous case, we obtain a separate decoupled system of linear equations for each wavenumber k_x. All of the physical quantities associated with a given wavenumber will have $\exp(-ik_x x)$ horizontal dependence. For an isotropic medium the tractions, σ_{iz}, on a boundary with a normal vector in the z direction are given by

$$\begin{aligned}\sigma_{yz} &= \mu \frac{du_y}{dz} \\ \sigma_{xz} &= \mu\left(\frac{du_x}{dz} - ik_x u_z\right) \\ \sigma_{zz} &= (\lambda + 2\mu)\frac{du_z}{dz} - ik_x \lambda u_x.\end{aligned} \tag{B1}$$

Eqs (B1) apply to a medium with the geometry shown in Fig. 1, for which u_y is the *SH* displacement and (u_x, u_z) is the *P–SV* displacement, but are not true in general. Note that σ_{yz} is the *SH* traction, and $(\sigma_{xz}, \sigma_{zz})$ is the *P–SV* traction.

For the medium in Fig. 1, eq. (8) becomes

$$\begin{aligned}&\sigma_{yz} - S_{yz}u_y = 0 \\ &\sigma_{xz} - S_{xx}u_x - S_{xz}u_z = 0 \\ &\sigma_{zz} - S_{zx}u_x - S_{zz}u_z = 0.\end{aligned} \tag{B2}$$

Combining eqs (B1) and (B2) we see that for the case shown in Fig. 1 the natural boundary condition, eq. (8), can be written

$$\begin{aligned}&\mu\frac{du_y}{dz} - S_{yz}u_y = 0 \\ &\mu\left(\frac{du_x}{dz} - ik_x u_z\right) - S_{xx}u_x - S_{xz}u_z = 0 \\ &(\lambda + 2\mu)\frac{du_z}{dz} - ik_x\lambda u_x - S_{zx}u_x - S_{zz}u_z = 0.\end{aligned} \tag{B3}$$

B1.1 SH problem

The general solution of the equation of motion for *SH* waves in an isotropic homogeneous region is

$$u_y(x, z) = [A\exp(ik_{z\beta}z) + B\exp(-ik_{z\beta}z)]\exp(-ik_x x), \tag{B4}$$

where A and B are constants, and $k_{z\beta} = (\omega^2/\beta^2 - k_x^2)^{1/2}$ is the vertical wavenumber. As z is positive in the downward direction, the first term of eq. (B4) corresponds to upgoing (incoming) waves and the second term corresponds to downgoing (outgoing) waves. A radiation boundary condition must forbid the existence of upgoing waves. We thus require

$$\frac{du_y}{dz} = -ik_{z\beta}u_y. \tag{B5}$$

Note that eq. (B5) is satisfied if and only if $A = 0$ in eq. (B4). Multiplying both sides of eq. (B5) by μ, we express the radiation boundary condition in the form of eq. (B3)

$$\mu\frac{du_y}{dz} + ik_{z\beta}\mu u_y = \mu\frac{du_y}{dz} - S_{yz}u_y = 0. \tag{B6}$$

We can see by inspection that $S_{yz} = -i\mu k_{z\beta}$.

B1.2 P–SV problem

In a homogeneous region the *P–SV* displacement can be derived from the potentials ϕ and ψ,

$$\begin{cases} u_x = \dfrac{\partial\phi}{\partial x} - \dfrac{\partial\psi}{\partial z} = -ik_x\phi - \dfrac{d\psi}{dz} \\ u_z = \dfrac{\partial\phi}{\partial z} + \dfrac{\partial\psi}{\partial x} = \dfrac{d\phi}{dz} - ik_x\psi, \end{cases} \tag{B7}$$

which obey the following wave equations

$$(\nabla^2 + \omega^2/\alpha^2)\phi = 0 \quad \text{and} \quad (\nabla^2 + \omega^2/\beta^2)\psi = 0, \tag{B8}$$

where α and β are, respectively, the compressional and the shear-wave velocities infinitesimally above the lower boundary at $z = R$. The radiation boundary conditions for the P and SV displacement potentials are, respectively,

$$\frac{d\phi}{dz} = -ik_{z\alpha}\phi \quad \text{and} \quad \frac{d\psi}{dz} = -ik_{z\beta}\psi \quad \text{at} \quad z = R. \tag{B9}$$

$k_{z\alpha}$ and $k_{z\beta}$ are the vertical wavenumbers for compressional waves and shear waves, respectively

$$\begin{cases} k_{z\alpha} = \left(\dfrac{\omega^2}{\alpha^2} - k_x^2\right)^{1/2} \\ k_{z\beta} = \left(\dfrac{\omega^2}{\beta^2} - k_x^2\right)^{1/2}. \end{cases} \tag{B10}$$

We use eq. (B9) to derive expressions for du_x/dz and du_z/dz in terms of u_x and u_z. We use the radiation condition, eq. (B9), to replace $d\phi/dz$ and $d\psi/dz$ in eq. (B7). We obtain

$$\begin{cases} u_x = -ik_x\phi + ik_{z\beta}\psi \\ u_z = -ik_{z\alpha}\phi - ik_x\psi. \end{cases} \tag{B11}$$

We solve for ϕ and ψ to obtain

$$\begin{cases} \phi = i\dfrac{k_x u_x + k_{z\beta} u_z}{k_x^2 + k_{z\alpha} k_{z\beta}} \\ \psi = i\dfrac{k_x u_z - k_{z\alpha} u_x}{k_x^2 + k_{z\alpha} k_{z\beta}}. \end{cases} \tag{B12}$$

Next, we re-state the radiation boundary conditions, eq. (B9), as constraints on du_x/dz and du_z/dz rather than $d\phi/dz$ and $d\psi/dz$. We obtain the following:

$$\begin{aligned} \frac{du_x}{dz} &= \frac{d}{dz}(-ik_x\phi + ik_{z\beta}\psi) \\ &= -ik_x\frac{d\phi}{dz} + ik_{z\beta}\frac{d\psi}{dz} \\ &= -k_x k_{z\alpha}\phi + k_{z\beta}^2\psi \\ &= Au_x + Bu_z, \end{aligned} \tag{B13}$$

where we differentiated both sides of eq. (B11) with respect to z, eliminated $d\phi/dz$ and $d\psi/dz$ using eq. (B9), and finally used eq. (B12). We follow the same basic procedure to obtain an expression for du_z/dz

$$\frac{du_z}{dz} = Cu_x + Du_z. \tag{B14}$$

The explicit values of the coefficients in eqs (B13) and (B14) are

$$\begin{aligned} A &= -i\frac{(k_x^2 + k_{z\beta}^2)k_{z\alpha}}{k_x^2 + k_{z\alpha}k_{z\beta}}, \quad B = -i\frac{k_x k_{z\beta}(k_{z\alpha} - k_{z\beta})}{k_x^2 + k_{z\alpha}k_{z\beta}} \\ C &= -i\frac{k_x k_{z\alpha}(k_{z\alpha} - k_{z\beta})}{k_x^2 + k_{z\alpha}k_{z\beta}}, \quad D = -i\frac{(k_x^2 + k_{z\alpha}^2)k_{z\beta}}{k_x^2 + k_{z\alpha}k_{z\beta}}. \end{aligned} \tag{B15}$$

Note that Spudich & Ascher (1983, eqs 21 and 22) derived similar results for cylindrical coordinates.

We use eqs (B15) and (B3) to derive the explicit form of the coefficients S_{ij}

$$\begin{aligned} \begin{bmatrix} S_{xx} & S_{xz} \\ S_{zx} & S_{zz} \end{bmatrix} &= \begin{bmatrix} A\mu & (B - ik_x)\mu \\ (C(\lambda + 2\mu) - ik_x\lambda) & D(\lambda + 2\mu) \end{bmatrix} \\ &= \begin{bmatrix} A\mu & -E\mu \\ E\mu & D(\lambda + 2\mu) \end{bmatrix}, \end{aligned} \tag{B16}$$

where we used the identity

$$\omega^2\rho = \mu(k_x^2 + k_{z\beta}^2) = (\lambda + 2\mu)(k_x^2 + k_{z\alpha}^2) \tag{B17}$$

to simplify the off-diagonal coefficients in eq. (B16), and where

$$E = \frac{ik_x(k_x^2 + 2k_{z\alpha}k_{z\beta} - k_{z\beta}^2)}{k_x^2 + k_{z\alpha}k_{z\beta}}. \tag{B18}$$

B2 Laterally heterogeneous media

We consider *SH*-wave propagation in the laterally heterogeneous domain shown in Fig. 4, where the strip just above the radiating lower boundary is homogeneous. We expand the wavefield at the lower boundary $z = R$ in terms of plane waves

$$u(x, R) = \sum_l A_l \exp(-ik_{xl}x) \tag{B19}$$

where $k_{xl} = l\pi/L$ and A_l is the amplitude of each plane-wave component.

The radiation boundary condition is, following eq. (B5)

$$\frac{\partial u}{\partial z} = \sum_l [-ik_{zl}A_l \exp(-ik_{xl}x)]. \tag{B20}$$

Since, as discussed in Appendix A, the horizontal dependence of our trial functions is already given by plane waves, we implement eq. (B20) by using $S_{ij} = -i\mu k_{zl}$ in eq. (40), where k_{zl} is the vertical wavenumber for the jth trial function. This makes eq. (B20) a natural boundary condition for eq. (37). This procedure can be extended to the case of trial functions which do not have their horizontal dependence given by plane waves, but details are not given here.